

# 3D Brain and Heart Volume Generative Models: A Survey

YANBIN LIU, Harry Perkins Institute of Medical Research, Department of Computer Science and Software Engineering, The University of Western Australia, Australia

GIRISH DWIVEDI\*, Harry Perkins Institute of Medical Research, The University of Western Australia, Fiona Stanley Hospital, Australia

FARID BOUSSAID, Department of Electrical, Electronic and Computer Engineering, The University of Western Australia, Australia

MOHAMMED BENNAMOUN, Department of Computer Science and Software Engineering, The University of Western Australia, Australia

Generative models such as generative adversarial networks and autoencoders have gained a great deal of attention in the medical field due to their excellent data generation capability. This paper provides a comprehensive survey of generative models for three-dimensional (3D) volumes, focusing on the brain and heart. A new and elaborate taxonomy of unconditional and conditional generative models is proposed to cover diverse medical tasks for the brain and heart: unconditional synthesis, classification, conditional synthesis, segmentation, denoising, detection, and registration. We provide relevant background, examine each task and also suggest potential future directions. A list of the latest publications will be updated on GitHub to keep up with the rapid influx of papers at <https://github.com/csyabin/3D-Medical-Generative-Survey>.

CCS Concepts: • **Computing methodologies** → **Computer vision; 3D imaging**.

Additional Key Words and Phrases: generative models, three-dimensional, medical images, brain and heart

## 1 INTRODUCTION

A wide range of research fields has embraced deep learning (DL) in recent years, including image processing [52, 63, 64, 97], speech recognition [57, 68, 128], natural language processing [22, 30, 90, 190, 203], and robotics [149, 189]. Thus, the medical imaging community has put in significant efforts to take advantage of deep learning advances, and medical imaging research has made significant progress with respect to a variety of applications including classification [14, 98, 153, 154, 245], segmentation [46, 121, 137, 195, 195], registration [160, 255], detection [150, 151, 197], denoising [161, 213, 214, 216, 252], and synthesis [34, 74, 78, 111, 119], as well as with various imaging modalities, including Computed Tomography (CT) [107, 217], ultrasound [117], Magnetic Resonance Imaging (MRI) [3, 123], and Positron Emission Tomography (PET) [163].

A large number of annotated training images, obtained with the aid of crowd-sourcing annotation platforms like Amazon Mechanical Turk [144], were required for deep learning to be successful in natural image processing. However, the complexity of collection procedures, the lack of experts, privacy concerns, and the mandatory requirement of consent from patients make the annotation process a major bottleneck in medical imaging. In order to mitigate this issue, deep generative models (e.g., generative adversarial networks (GANs) [55] and variational autoencoder (VAE) [92]) have been introduced to medical imaging. In these generative models, the original data distribution

---

\*This work was supported by MRFF Frontier Health and Medical Research - RFRHPI000147.

---

Authors' addresses: Yanbin Liu, [csyanbin@gmail.com](mailto:csyanbin@gmail.com), Harry Perkins Institute of Medical Research, Department of Computer Science and Software Engineering, The University of Western Australia, Canberra, ACT, Australia, 2601; Girish Dwivedi, Harry Perkins Institute of Medical Research, The University of Western Australia, Fiona Stanley Hospital, Perth, WA, Australia, [girish.dwivedi@perkins.uwa.edu.au](mailto:girish.dwivedi@perkins.uwa.edu.au); Farid Boussaid, Department of Electrical, Electronic and Computer Engineering, The University of Western Australia, Perth, WA, Australia, [farid.boussaid@uwa.edu.au](mailto:farid.boussaid@uwa.edu.au); Mohammed Bennamoun, Department of Computer Science and Software Engineering, The University of Western Australia, Perth, WA, Australia, [mohammed.bennamoun@uwa.edu.au](mailto:mohammed.bennamoun@uwa.edu.au).

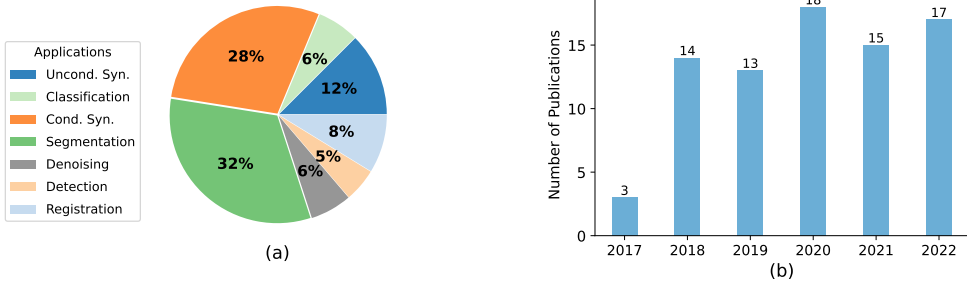


Fig. 1. Statistics of the 3D brain and heart volume generative models. (a) Statistics of all publications according to medical applications. (b) Categorization by year of publication (2017-2022). Uncond. Syn.: Unconditional Synthesis, Cond. Syn.: Conditional Synthesis.

is mimicked so that realistic images are generated [74, 188, 207] or cross-modality synthesis can be achieved [111, 114, 237].

There have been numerous survey papers published on deep generative models for medical imaging due to the rapid progress of the field [4, 5, 21, 79, 83, 89, 219, 234]. These surveys cover different medical applications and provide an overall review of GANs on general medical image analysis [4, 89, 234]. Some focus on a specific application only, such as augmentation [21], segmentation [79, 83] and registration [219]. Others concentrate on a specific image modality, such as MRI [5]. Even though many surveys exist, we find that there is a lack of comprehensive surveys on three-dimensional (3D) medical volume, which is the original data format of many medical modalities, such as MRI, CT, and PET. Moreover, existing surveys mainly focus on GANs, neglecting other effective generative models such as Autoencoders (AEs) [67] and Autoregressive models [202]. In Section 2.1, we provide a comprehensive comparison to existing survey papers in the field of medical image generation (as shown in Table 1) and detail what sets our survey apart.

This inspired us to conduct a comprehensive survey of generative models for 3D medical volume images of the brain and heart. Since 3D volume is the intrinsic representation of many medical imaging modalities, it displays the entire and thorough anatomical structure of organs, whereas a 2D medical image only shows a specific view/plane. GANs are widely used for 3D medical volumes, but there has also been an increased interest in AEs (e.g., Diffusion Model [91, 150]) and Autoregressive models (e.g., Autoregressive Transformers [151]). As a result, our survey covers all three types of generative models. As far as organs are concerned, we restrict our interest to the brain and heart for the following reasons: (1) they are two vital organs that control the mental and physiological functions of the human body; (2) both organs involve a wide range of applications, e.g., segmentation (Fig. 1(a)); (3) generative models are essential for both organs because of their data scarcity; (4) by covering these 2 organs, we are able to cover generative models for both static (i.e., brain) and dynamic organs (i.e., heart).

**Contributions.** To provide a comprehensive and organized survey, we introduce a new taxonomy (Fig. 2) that divides generative models into unconditional (only taking a random variable as input) and conditional (taking an additional data modality as input). In Figure 1, we provide a statistical analysis of the proportion of publications per application and the number of publications per year. Our contributions can be summarized as follows:

- This is the *first survey* on generative models for 3D medical volume images, focusing on two important organs, i.e., the brain and the heart. It aims to bridge the gap between the

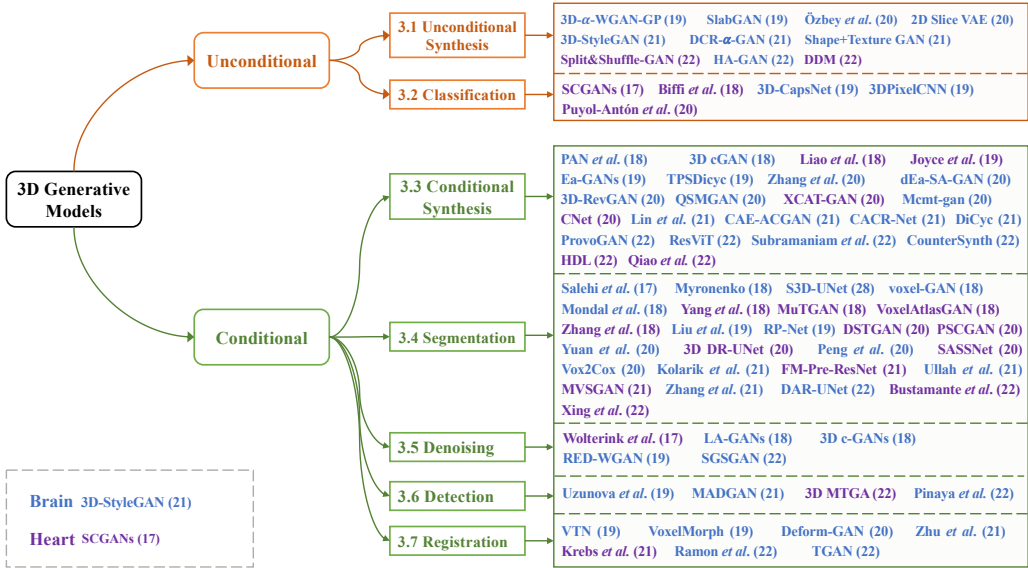


Fig. 2. Proposed taxonomy of 3D generative models for the brain and the heart. The numbers in the parentheses denote the publication year (after 2000).

research of the 3D generative models community and the research of the medical imaging community.

- We provide a new taxonomy (Fig. 2) of 3D generative models by categorizing them as unconditional or conditional generative models. Every category includes several relevant medical applications.
- Whilst most existing surveys focus on GANs only, we cover three main categories of generative models: GANs, AEs, and Autoregressive models.
- We discuss the key challenges and future directions of 3D medical generative models and applications.

**Paper Organization.** The remainder of this paper is organized as follows. We introduce the foundational techniques and challenges of 3D generative models in Section 2. Section 3 comprehensively elaborates on the 3D medical applications of both the unconditional and conditional generative models, including unconditional synthesis, classification, conditional synthesis, segmentation, denoising, detection, and registration. Then, Section 4 discusses the above-surveyed applications and gives four future directions. Finally, Section 5 concludes the paper.

## 2 BACKGROUND

### 2.1 Related Survey

As generative models find increasing use in the medical field, many survey papers have been published to provide overviews [4, 5, 21, 79, 89, 234]. In Table 1, we differentiate our survey from existing ones by comparing key elements such as Model(s), Organ(s), Image Format, and Application(s). The distinct contributions and unique aspects of our survey are summarized below:

Table 1. Comparison with existing survey papers on medical image generation.

Publication	Year	Model(s)	Organ(s)	Image Format	Application(s)
Yi <i>et al.</i> [234]	2019	GANs	All	mainly 2D, 3D	synthesis, reconstruction, segmentation, classification detection, registration
Kazemina <i>et al.</i> [89]	2020	GANs	All	mainly 2D, 3D	synthesis, segmentation, reconstruction, detection de-noising, registration, classification
ALAMIR <i>et al.</i> [4]	2022	GANs	All	mainly 2D, 3D	cross-modality, segmentation, augmentation, reconstruction detection, classification, registration
Chen <i>et al.</i> [21]	2022	GANs	All	2D, 3D	augmentation
Iqbal <i>et al.</i> [79]	2022	GANs	All	2D, 3D	segmentation
Jeong <i>et al.</i> [83]	2022	GANs	All	mainly 2D, 3D	classification, segmentation
Ali <i>et al.</i> [5]	2022	GANs	Brain	2D, 3D	only statistics of all applications (no description)
This Survey	2023	GANs, AEs Autoregressive	Brain, Heart	focus on 3D	unconditional synthesis, classification, conditional synthesis segmentation, denoising, detection, registration

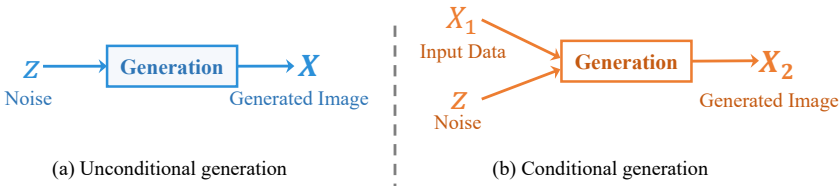


Fig. 3. Generation process in unconditional and conditional generative models.

- While the majority of existing surveys concentrate on Generative Adversarial Networks (GANs), our survey includes all three major types of generative models: GANs, Autoencoders (AEs), and Autoregressive models. Notably, a recent AE variant, Denoising Diffusion Probabilistic Models (DDPMs) [70], has outperformed GANs in the generation of natural images [40, 71]. Additionally, Autoregressive Transformer [47] has shown promise in generating high-resolution images. Both AEs and Autoregressive models are poised to make significant contributions to medical image generation in the near future.
- We observed that there is a gap in the literature when it comes to survey papers focused specifically on brain and heart image generation. While Ali *et al.* [5] do cover brain MRI, their scope is limited to providing general statistics on demographics, applications, evaluations, and datasets. To our knowledge, no survey exists that focuses on heart image generation. Our survey aims to fill this gap.
- Given that GANs were initially developed for 2D images, several existing surveys [4, 83, 89, 234] primarily focus on 2D generative models. In contrast, our survey focuses on 3D volumes, the native image format for medical imaging. Utilizing this 3D format offers additional advantages for subsequent applications [74, 119].

## 2.2 Unconditional and Conditional Generative Models

In this paper, we divide generative models for 3D volume images into two categories: unconditional model and conditional model (Fig. 3), where we only show the generation process for simplicity.

In an unconditional generative model (Fig. 3(a)), the input is a random noise variable  $z$ , and the output from the generation model is the generated image  $X$ . Several model architectures belong to this type of model. A GAN generator, for example, only uses random noise variables to synthesize images. Random Gaussian variables are input to the decoder of the VAE model. The unconditional generative model is used in several 3D medical applications, including unconditional synthesis [74, 100, 119, 207] and classification [14, 102, 153].

In a conditional generative model (Fig. 3(b)), in addition to the random noise  $z$ , the informative input data  $X_1$  (e.g., semantic or visual input) is also fed to the generation model to help generate the output image  $X_2$ . Depending on the applications, a variety of data formats are supported by  $X_1$ , including class labels [130], attributes [229], texts [164], and images [81]. For example, the original cGAN [130] generated synthetic MNIST [105] images conditioned on the class labels. Pixel-to-pixel [81] achieved image style transfer by training a conditional GAN whose generator and discriminator were both based on the input images. Many 3D medical applications take advantage of the conditional generative model, including conditional synthesis [34, 111, 143, 152, 231, 235, 236], segmentation [28, 165, 165, 242, 247], denoising [161, 213, 214, 216, 252], detection [61, 151, 197, 224], and registration [11, 160, 246, 250, 254].

From the data distribution perspective, the unconditional generative model captures the original realistic data distribution without requiring any additional information other than random noise. The conditional generative model can be regarded as a transformation from the input data distribution  $p(X_1)$  to the output image distribution  $p(X_2)$ . By proposing a new unconditional/conditional taxonomy perspective, we hope researchers can gain valuable insights into future model design and apply them to target medical applications in the future.

### 2.3 Generative Adversarial Networks

Generative Adversarial Networks were proposed by Goodfellow *et al.* [55] in 2014. The main idea is to design two networks (a discriminator and a generator) to contest with each other in a zero-sum two-layer game. Specifically, the generator  $G$  takes a random noise variable  $z$  as the input to generate the synthesized images  $G(z)$ . The role of the discriminator is to distinguish between the realistic images  $x$  and the generated fake images  $G(z)$ . In an ideal case, the two-player game reaches a Nash equilibrium [48, 66] where the synthesized images  $G(z)$  are indistinguishable from real images  $x$ . The equilibrium is difficult to achieve in practice, and GANs training suffers from two problems, i.e., training instability [173, 191] and mode collapse [184, 192]. Diverse architectures and training strategies have been proposed to address the two problems and improve GANs performance [69, 172, 248, 251]. Below, we describe the variants that are most relevant to the generation of 3D medical volume images.

**2.3.1 Vanilla GAN.** The structure of the vanilla GAN is shown in Fig. 4(a). Based on a prior distribution of the input noise variable  $z \sim p_z(z)$ , the generator trains its distribution  $p_g$  over  $x$  to approximate the real data distribution  $p_{data}$ . The discriminator maximizes the accuracy of classifying real/fake images by optimizing over  $D(x)/D(G(z))$ . The minmax optimization problem for  $G$  and  $D$  is defined as follow:

$$\min_G \max_D V(D, G) = \mathbb{E}_{x \sim p_{data}(x)} [\log D(x)] + \mathbb{E}_{z \sim p_z(z)} [\log(1 - D(G(z)))] . \quad (1)$$

Theoretically, for arbitrary functions  $G$  and  $D$ , the optimal solution satisfies  $p_g = p_{data}$  and  $D(x) = D(G(z)) = \frac{1}{2}$ . But in practice,  $G$  and  $D$  are usually implemented by deep neural networks (e.g., multilayer perceptrons or convolution neural networks), which only have limited capacity and cover a limited family of  $p_g$  distributions.

**2.3.2 Conditional GAN.** The vanilla GAN is unconditional, which means it cannot use additional information or control the modes of the generated data. Hence, conditional GAN (cGAN) [130] was proposed in order to improve the flexibility of vanilla GAN by conditioning on additional information. As shown in Fig. 4(b), the conditional input  $c$  is fed into both the generator  $G$  and discriminator  $D$  (red line). The minmax optimization problem for  $D$  and  $G$  is then defined as follow:

$$\min_G \max_D V(D, G) = \mathbb{E}_{x \sim p_{data}(x)} [\log D(x|c)] + \mathbb{E}_{z \sim p_z(z)} [\log(1 - D(G(z|c)))] . \quad (2)$$

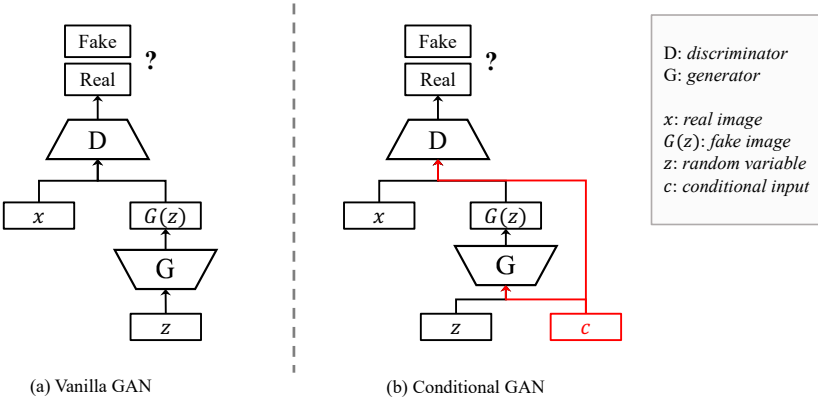


Fig. 4. The structure of (a) the vanilla (unconditional) and (b) the conditional GAN.

The conditional GAN (Eq. 2) is different from the unconditional GAN (Eq. 1) because it conditions on  $c$  in the generation and discrimination process.  $c$  is used in the original paper [130] to represent labels in the MNIST [105] image generation and to represent image features in the generation of multi-model Flickr tags.

The conditional input  $c$  can be instantiated with different information and modalities so as to perform various image generation tasks. These tasks include text-to-image synthesis [243, 244], image-to-image translation [81, 253], attribute editing [148, 229], image segmentation [46, 195], etc.

**2.3.3 Pixel-to-pixel.** Pixel-to-pixel was proposed in [81] to solve the general image-to-image translation problems, e.g., edge to photo, day to night. In its implementation, both the generator and discriminator are fed with input images to construct a conditional GAN architecture. The objective function is as follows:

$$\min_G \max_D \mathbb{E}_{x,y} [\log D(x, y)] + \mathbb{E}_{x,z} [\log(1 - D(x, G(x, z)))] + \lambda \mathbb{E}_{x,y,z} [\|y - G(x, z)\|_1]. \quad (3)$$

Pixel-to-pixel is trained with image pairs  $(x, y)$ , and translates images from  $x$  domain to  $y$  domain after training.

**2.3.4 CycleGAN.** Since Pixel-to-pixel [81] relies on a large number of annotated image pairs, it is time-consuming and sometimes infeasible. CycleGAN [253] tackles this problem by taking advantage of the concept of cycle-consistency. Two discriminators  $G$  and  $F$  are designed for forward and backward mapping, and two discriminators  $D_X$  and  $D_Y$  are devised for adversarial learning. The objective function is as follows:

$$L(G, F, D_X, D_Y) = L_{GAN}(G, D_Y, X, Y) + L_{GAN}(F, D_X, Y, X) + \lambda L_{cyc}(G, F), \quad (4)$$

where  $L_{GAN}$  is the adversarial loss, and  $L_{cyc}$  is the cycle-consistency loss.

**2.3.5 WGAN and WGAN-GP.** The GANs training objective can be non-continuous with respect to the generator parameters, resulting in training instability. To alleviate this issue, Wasserstein GAN (WGAN) [8] was proposed to leverage the Wasserstein distance as its objective function. To further improve the training stability and generation quality, [59] designed WGAN-GP, a GAN variant, by adding the gradient penalty in the WGAN training loss. The WGAN-GP objective function is:

$$L = \mathbb{E}_{\hat{x} \sim p_g} [D(\hat{x})] - \mathbb{E}_{\mathbf{x} \sim p_{data}} [D(\mathbf{x})] + \lambda \mathbb{E}_{\hat{x} \sim p_{\hat{x}}} [(\|\nabla_{\hat{x}} D(\hat{x})\|_2 - 1)^2], \quad (5)$$

where  $\hat{x}$  are random samples used to calculate the gradient.

**2.3.6 StyleGAN and StyleGAN2.** A style-based generative model, such as StyleGAN [87], uses a mapping network to produce style vectors for each convolution layer of the generator. In StyleGAN, the Adaptive Instance Normalization (AdaIN) operation takes the style vectors as input to control the generation style. With this method, diverse and high-quality images can be generated with good interpolation properties. For example, style vectors corresponding to specific attributes can be jointly utilized to generate images of desired attributes, such as pose, skin tone, and hairstyle. However, StyleGAN suffers from characteristic artifacts (e.g., water droplet-like artifacts), which are corrected by the improved StyleGAN2 [88] model. By design, StyleGAN2 designed the modulation and demodulation modules to incorporate style vectors into the convolution operation. Moreover, it proposed lazy regularization and alternative network designs (i.e., input/output skips and residual nets). As a result of its good performance, the StyleGAN2 model has been used in a wide range of medical imaging methods [74, 119].

## 2.4 Autoencoders

The concept of autoencoder dates back to the early stages of neural networks [16, 67, 104]. The original purpose of AEs was to perform dimensionality reduction or feature learning in an unsupervised manner. An autoencoder is composed of an encoder  $E$  with parameter  $\phi$  and a decoder  $D$  with parameter  $\theta$ . Typically, an autoencoder has a bottleneck structure (a.k.a undercomplete), i.e., the latent embedding dimension of the encoder is smaller than the original data  $x$ . With this design, the autoencoder can capture the intrinsic features of the data. The training of an autoencoder can be achieved by minimizing the reconstruction error (e.g., mean squared error) as follows:

$$\min_{\theta, \phi} \mathbb{E}_x \|x - D_{\theta}(E_{\phi}(x))\|^2. \quad (6)$$

With the recent emergence of deep neural networks, a multitude of AE model variants have been developed, such as Denoising Autoencoder (DAE) [205, 206], VAE [92], conditional VAE [159, 183], VQVAE [199], and U-Net [168]. We cover below the most relevant AE models for the synthetic generation of 3D medical volume images.

**2.4.1 Variational Autoencoder (VAE).** Synthetic image generation was not the primary goal of the original autoencoder, which instead focused on feature learning or dimensionality reduction. The VAE [92] introduced a new generative model by combining the AE structure and the variational inference technique. As shown in Fig. 5, the input data  $x$  is encoded to a Gaussian distribution  $\mathcal{N}(x; \mu_x, \sigma_x^2)$  with the Encoder  $E_{\phi}(x)$ . Then, a variable  $z$  is sampled from the Gaussian  $z \sim \mathcal{N}(\mu_x, \sigma_x^2)$ . Finally, the decoder  $D_{\theta}(z)$  takes  $z$  to generate the reconstructed data  $\tilde{x}$ . The intuition behind the VAE is to encode an input as a distribution instead of a simple point. With proper regularization of the distribution, the latent space of the VAE becomes more continuous and complete and can therefore be conveniently sampled to improve the quality of the data generation.

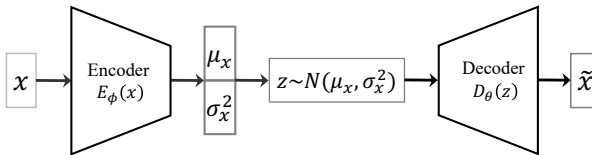


Fig. 5. The structure of Variational Autoencoder (VAE).

For effective training of the VAE model, the following Evidence lower bound (ELBO) is optimized:

$$\log p_{\theta}(x) \geq \mathcal{L}(\theta, \phi; x) = -D_{KL}(q_{\phi}(z|x) || p_{\theta}(z)) + \mathbb{E}_{q_{\phi}(z|x)} [\log p_{\theta}(x|z)], \quad (7)$$



where  $q_\phi(\mathbf{z}|\mathbf{x})$  is a model used to approximate the intractable posterior distribution  $p_\theta(\mathbf{z}|\mathbf{x})$ ,  $D_{KL}$  is the Kullback–Leibler divergence between two distributions to measure the divergence between two distributions, and  $p_\theta(\mathbf{x}|\mathbf{z})$  is the reconstruction probability of  $\mathbf{x}$  given  $\mathbf{z}$ . In a deep VAE framework (Fig. 5),  $q_\phi(\mathbf{z}|\mathbf{x})$  is modeled by an Encoder  $E_\phi(\mathbf{x})$  and  $p_\theta(\mathbf{z}|\mathbf{x})$  is modeled by a Decoder  $D_\theta(\mathbf{z})$ .  $p_\theta(\mathbf{z})$  is set to an isotropic Gaussian to regularize the posterior distribution. Moreover, the reparameterization trick is used to facilitate the model training and the gradient estimation:  $\mathbf{z} = \mu_x + \sigma_x \epsilon$ ,  $\epsilon \sim \mathcal{N}(0, 1)$ .

**2.4.2 Conditional VAE (CVAE).** Similar to the Conditional GAN, a conditional version of the VAE model was proposed in [183]. The model is not trained to reconstruct the input  $\mathbf{x}$ . Instead, for the input  $\mathbf{x}$ , the latent variable  $\mathbf{z}$  is sampled from  $p_\theta(\mathbf{z}|\mathbf{x})$ , and then a different output  $\mathbf{y}$  is generated according to  $p_\theta(\mathbf{y}|\mathbf{x}, \mathbf{z})$  rather than the original reconstruction  $\tilde{\mathbf{x}}$ . Based on the ELBO of the VAE, the variational lower bound of this conditional model is as follows:

$$\log p_\theta(\mathbf{y}|\mathbf{x}) \geq -D_{KL}(q_\phi(\mathbf{z}|\mathbf{x}, \mathbf{y})||p_\theta(\mathbf{z}|\mathbf{x})) + \mathbb{E}_{q_\phi(\mathbf{z}|\mathbf{x}, \mathbf{y})}[\log p_\theta(\mathbf{y}|\mathbf{x}, \mathbf{z})]. \quad (8)$$

For a deep CVAE framework,  $q_\phi(\mathbf{z}|\mathbf{x}, \mathbf{y})$  is modeled as a recognition network,  $p_\theta(\mathbf{z}|\mathbf{x})$  is modeled as a conditional prior network, and  $p_\theta(\mathbf{y}|\mathbf{x}, \mathbf{z})$  is modeled as the generation network. All these networks can be either Multi-Layer Perceptrons (MLPs) or Convolution Neural Networks (CNNs).

Various applications can be derived from different choices of  $\mathbf{x}$  and  $\mathbf{y}$ . For example, if  $\mathbf{x}$  represents the original image and  $\mathbf{y}$  represents the segmentation mask, then we are dealing with an image segmentation task. If  $\mathbf{x}$  represents an MRI image and  $\mathbf{y}$  represents a CT image, then we are dealing with an MRI-to-CT translation task.

**2.4.3 U-Net.** U-Net was first proposed in [168] for biomedical image segmentation. It has an encoder-decoder architecture, as shown in Figure 6. Specifically, the encoder converts an image  $X$  into a lower-dimension representation. Then, the decoder takes these representations as inputs and copies several intermediate feature maps from the encoder to generate the segmentation mask  $Y$ . Due to its excellent performance, U-Net has been widely used in medical applications besides segmentation, including cross-modality synthesis [43], registration [11, 246, 250], etc. For 3D medical applications, the 3D U-Net [27] was designed by using 3D convolution to process the 3D volume images. Moreover, the U-Net design can also be used as the main structure of other generative models, e.g., the U-Net generator in GANs.

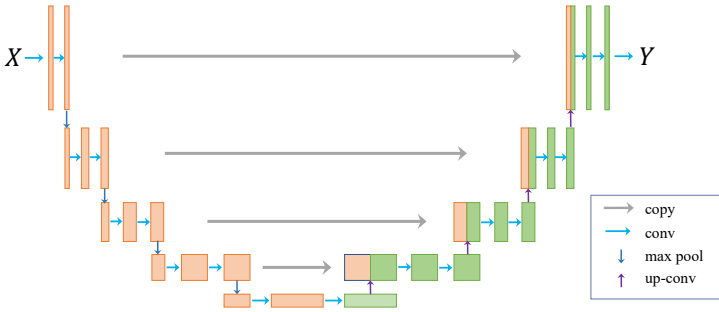


Fig. 6. A schematic view of the U-Net architecture. Several intermediate feature maps from the encoder are copied and concatenated in the decoder.



**2.4.4 Denoising Autoencoder (DAE).** DAE [206] is an autoencoder that takes in the corrupted data at the input to reconstruct the original uncorrupted data. A noise function  $T : \mathcal{X} \rightarrow \mathcal{X}$  is applied on the data  $x \in \mathcal{X}$  of a standard autoencoder to construct a DAE. The objective of a DAE is to reconstruct the original data  $X$  from the noisy input  $T(x)$ . Thus, the following optimization problem can be defined:

$$\min_{\theta, \phi} \mathbb{E}_x \|x - (D_\phi \circ E_\theta \circ T)(x)\|^2. \quad (9)$$

In a similar way to the bottleneck design, the denoising training strategy can facilitate the learning of the inherent features of the original data. Besides the manually designed noise function  $T$ , certain medical image collection and processing devices can produce noisy and low-quality medical images, e.g., low-dose CT images. In this case, the idea of DAE can be applied to the medical image denoising task [1, 54].

**2.4.5 Structural Causal Models (SCMs).** To integrate causality into deep learning methods for improved interpretability, deep structural causal models (Deep SCMs) [145] incorporated deep learning components into SCMs. Given the random variable  $\mathbf{x}$  and noise variable  $\epsilon$ , an SCM  $\mathcal{B} := (\mathbf{S}, P(\epsilon))$  can be constructed with *mechanisms*  $\mathbf{S} = (f_1, \dots, f_k)$  and  $x_k := f_k(\epsilon_k; \text{pa}_k)$ , where  $\text{pa}_k$  is the parents of  $x_k$  (*direct causes*). Three types of deep mechanisms can be implemented: 1) invertible explicit likelihood with normalizing flow:  $f_i(\epsilon_i; \text{pa}_i), p(x_i | \text{pa}_i) = p(\epsilon_i) \cdot |\det_{\epsilon_i} f_i(\epsilon_i; \text{pa}_i)|^{-1} |_{\epsilon_i=f_i^{-1}(x_i; \text{pa}_i)}$ ; 2) amortized explicit likelihood with variational inference:  $f_k(\epsilon_k; \text{pa}_k) = h_k(\mu_k; g_k(z_k; \text{pa}_k), \text{pa}_k)$ ,  $P(\epsilon_k) = P(\mu_k)P(z_k)$ , where  $h_k$  is invertible and  $g_k$  is non-invertible; 3) amortized implicit likelihood: use adversarial objective to train a conditional implicit model. With the deep mechanism, counterfactual inference can be performed in three steps: Abduction, Action, and Prediction. Several recent works explored the idea of interpretable models and counterfactual augmentation [14, 152, 154].

**2.4.6 Denoising Diffusion Probabilistic Model (DDPM).** Inspired by non-equilibrium thermodynamics [182], diffusion models devise a Markov chain of diffusion steps by gradually adding noise to the data (forward) and learning how to reverse the diffusion process (reverse) so that an image can be generated from the noise. Recent research has demonstrated that Denoising Diffusion Probabilistic Models (DDPMs) [70] outperform GANs in terms of natural image synthesis [40, 71]. Given data sample  $\mathbf{x}_0 \sim q(\mathbf{x}_0)$ , the forward diffusion process is defined as:  $q(\mathbf{x}_t | \mathbf{x}_{t-1}) = \mathcal{N}(\mathbf{x}_t; \sqrt{1 - \beta_t} \mathbf{x}_{t-1}, \beta_t \mathbf{I})$ ;  $q(\mathbf{x}_{1:T} | \mathbf{x}_0) = \prod_{t=1}^T q(\mathbf{x}_t | \mathbf{x}_{t-1})$ , where  $\beta_t$  controls the noise schedule such that  $q(\mathbf{x}_T | \mathbf{x}_0) \approx \mathcal{N}(\mathbf{x}_T; \mathbf{0}, \mathbf{I})$ . In other words, the forward process converts a data sample into a zero-mean isotropic Gaussian. The reverse denoising process is defined as:  $p(\mathbf{x}_T) = \mathcal{N}(\mathbf{x}_T; \mathbf{0}, \mathbf{I})$ ;  $p_\theta(\mathbf{x}_{t-1} | \mathbf{x}_t) = \mathcal{N}(\mathbf{x}_{t-1}; \mu_\theta(\mathbf{x}_t, t), \sigma_t^2 \mathbf{I})$ , where  $\mu_\theta(\mathbf{x}_t, t)$  is a trainable network to estimate the mean and  $\sigma_t^2$  is the variance schedule. The reverse process generates realistic data from Gaussian noise.

Similar to VAE, the training of the DDPM model uses the variational upper bound to construct the following objective function:

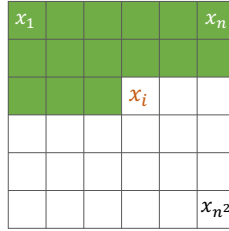
$$L = \mathbb{E}_q \left[ \underbrace{D_{KL}(q(\mathbf{x}_T | \mathbf{x}_0) \| p(\mathbf{x}_T))}_{L_T} + \sum_{t>1} \underbrace{D_{KL}(q(\mathbf{x}_{t-1} | \mathbf{x}_t, \mathbf{x}_0) \| p_\theta(\mathbf{x}_{t-1} | \mathbf{x}_t))}_{L_{t-1}} - \underbrace{\log p_\theta(\mathbf{x}_0 | \mathbf{x}_1)}_{L_0} \right]. \quad (10)$$

To improve the training of the objective function, a simplified version of  $L_{t-1}$  is proposed in [70]:  $L_{\text{simple}} = \mathbb{E}_{\mathbf{x}_0 \sim q(\mathbf{x}_0), \epsilon \sim \mathcal{N}(\mathbf{0}, \mathbf{I}), t \sim \mathcal{U}(1, T)} [\|\epsilon - \epsilon_\theta(\sqrt{\bar{\alpha}_t} \mathbf{x}_0 + \sqrt{1 - \bar{\alpha}_t} \epsilon, t)\|^2]$ . Here,  $\epsilon_\theta$  is a function approximator to predict  $\epsilon$  from  $\mathbf{x}_t$ , and  $\bar{\alpha}_t = \prod_{s=1}^t (1 - \beta_s)$ .  $L_{\text{simple}}$  achieved better generation quality on natural image benchmarks.

In practice, the approximation functions  $\mu_\theta(\mathbf{x}_t, t)$  or  $\epsilon_\theta$  can be implemented with U-net or DAE structures. Due to the good generation performance, DDPM has been adopted in several recent medical imaging papers [91, 150].

## 2.5 Autoregressive Models

The hallmark problem of generative models is to model the distribution of images. GANs apply an adversarial strategy to indirectly approach the real distribution, while VAE employs variational inference to approximate it. In contrast, Autoregressive models [58, 202] explicitly compute the joint distribution of pixels by factorizing it into products of conditional distributions. As shown in Fig. 7, an  $n \times n$  image is represented by a sequence of pixels  $x_1, x_2, \dots, x_{n^2}$  according to the raster scan order<sup>1</sup>. The distribution of the forthcoming pixel  $x_i$  depends on the above and left surrounding pixels, i.e.,  $p(x_i|x_1, \dots, x_{i-1})$ . In order to calculate the distribution of the whole image, the chain rule is applied:  $p(x) = \prod_{i=1}^{n^2} p(x_i|x_1, \dots, x_{i-1})$ . For a color image, each pixel  $x_i$  is determined by three channels: Red, Green, and Blue. This is followed by the introduction of the successive dependency:  $p(x_i|\mathbf{x}_{<i}) = p(x_{i,R}|\mathbf{x}_{<i})p(x_{i,G}|\mathbf{x}_{<i}, x_{i,R})p(x_{i,B}|\mathbf{x}_{<i}, x_{i,R}, x_{i,G})$ .



$$p(x) = \prod_{i=1}^{n^2} p(x_i|x_1, \dots, x_{i-1})$$

Fig. 7. A schematic illustration of an autoregressive model. An image distribution is modeled as the distribution of all pixels, where each pixel is conditioned on the left and above surrounding pixels.

Autoregressive models calculate the tractable image distribution in an explicit and straightforward manner by maximizing the log-likelihood function. However, due to the factorization of multiple product terms, the direct computation is inefficient. Thus, a variety of autoregressive models [47, 58, 198, 202] have been proposed to enable fast and parallel computation. Below, we introduce several methods that are relevant to the synthetic generation of 3D medical volume images.

**2.5.1 PixelRNN and PixelCNN.** In order to improve the expressive power and efficiency of early autoregressive models such as NADE [103], the work in [202] used Recurrent Neural Networks (RNNs) to construct the PixelRNN model for large-scale natural image generation. PixelRNN is designed to stack multiple 2D Long Short-Term Memory (LSTM) layers. In each layer, there is a fixed input-to-state component and a recurrent state-to-state component to jointly compute the states and gates of an LSTM. Specifically, two types of LSTM layers are designed to implement the state-to-state components: Row LSTM and Diagonal BiLSTM. The Row LSTM processes the image row by row with a  $k \times 1$  convolution, while the Diagonal BiLSTM skews each input row by one position and processes with a  $2 \times 1$  convolution. Residual connections [64] are deployed to facilitate deep PixelRNN training.

The Row LSTM and the Diagonal BiLSTM have the benefit of potentially unbounded dependency range to model the global pixel correlations. However, they introduce large computation costs. Therefore, another variant (called PixelCNN) using standard convolution layers along with masks was proposed to enable a fast and parallel training process. The speedup of PixelCNN, however, degrades the generation performance when compared with the PixelRNN model.

<sup>1</sup>Rater scan order: row by row and pixel by pixel within every row

**2.5.2 Autoregressive Transformer.** Compared with RNNs and CNNs, Transformers [203] have shown superior performance in modeling the long-range interactions within sequences. This inspired the Autoregressive Transformer proposed in [47]. Specifically, a Vector Quantised GAN (VQGAN) was designed to learn a representative codebook from the patches of the training images. The composition of the codes in an image was then modeled using an autoregressive transformer. Finally, image generation was formulated as the autoregressive prediction of the next image patch, similar to PixelRNN. Conditional synthesis was also achieved in [47] by enforcing the conditional information in the autoregressive transformer.

## 2.6 Advantages and Disadvantages of Different Generative Models

GANs have become a preferred choice for medical image generation, offering multiple advantages such as (1) *High-Quality Output*: They are capable of generating highly realistic synthetic images, as evidenced by their top-tier FID scores [66], which can be used to augment limited medical image datasets. (2) *Flexibility*: Their versatility allows them to be applied to a variety of tasks, including image augmentation, segmentation, super-resolution, and denoising. (3) *Unpaired Cross-Modality Synthesis*: With the use of CycleGAN [253], GANs can convert between different imaging modalities like MRI to CT without requiring paired data, thereby reducing data collection burdens. Despite these benefits, GANs also have notable drawbacks, including (1) *Training Challenges*: They are notoriously difficult to train due to issues like training instability [173, 191] and mode collapse [184, 192], which arise from the oscillatory behavior of the two competing networks and vanishing gradients. (2) *Uninterpretable Latent Space*: The lack of an explicit latent space makes it challenging to interpret the patterns in the generated images, limiting their applicability in clinical decision-making.

While AEs may not match GANs in terms of generation quality, they offer their own set of advantages and can address some of GANs' limitations in specific contexts. These advantages include (1) *Latent Space Representation*: AEs feature an explicit latent space that facilitates representation learning and feature interpretation. (2) *Stable Training*: The use of reconstruction loss and regularization contributes to a more stable training process. (3) *Reconstruction Capability*: AEs are naturally suited for tasks like medical image denoising due to their reconstruction properties. However, AEs also come with their own set of drawbacks, such as (1) *Blurred Output*: The averaging effect in the latent space often results in less sharp images, particularly in models like VAEs. (2) *Limited Expressivity*: The constrained dimensionality of the latent space can limit the model's ability to generate high-dimensional data distributions.

Autoregressive models may be less common than GANs and AEs, but they excel as sequential generators. Their strengths include (1) *Explicit Distribution*: These models explicitly learn the joint distribution of pixels, enhancing both transparency and interoperability. (2) *Sequential Processing*: They are particularly effective for generating medical time-series data, such as 4D spatio-temporal anatomy [157], spatio-temporal registration [96], or Time-of-Flight [26]. However, their sequential nature also introduces some drawbacks, including (1) *Inefficient Parallelization*: The sequential architecture creates dependencies between pixels, making the training process slower. (2) *Absence of Latent Space*: Unlike GANs and AEs, autoregressive models do not have a latent feature space.

In the field of medical imaging, the choice of model is contingent on both the specific application and its requirements. For instance, GANs are generally the preferred choice when high-quality generation or cross-modality capabilities are needed. On the other hand, AEs are more suitable when the focus is on reconstruction or interpretability. For tasks involving sequential imaging data, Autoregressive models naturally come to the forefront. To aid readers in making an informed model selection, Section 3 provides a comprehensive list of models used in various papers and applications.

## 2.7 Challenges of 3D Generative Models

The aforementioned generative models have been applied to various two-dimensional (2D) tasks, including natural image generation [87, 88], image style transfer [81, 253], text-to-image generation [164], medical slice synthesis [4], 2D cross-modality synthesis [177, 249], etc. However, as a result of the intrinsic 3D nature of medical volume images, there are practical challenges that are beyond the design and training of 2D generative models.

**Insufficient 3D medical volumes for training.** A 2D generative model relies on a large number of readily accessible images (e.g., natural images, slices of medical volume images) in order to model real data distributions. For example, the widely-used ImageNet [38] dataset contains 1.28 million natural images. In the medical field, a big dataset for training can be created by compiling all the 2D slices of a 3D volume. Comparatively, 3D medical datasets are several orders of magnitude smaller. 3Dseg-8 [18] consists of eight medical datasets, with each dataset containing only tens to hundreds of volume images. For the training of generative models, [100] utilized only 991 brain T1-weighted image volumes from ADNI [215].

**3D model parameters.** 3D generative models usually utilize 3D convolution architectures, such as 3D-U-Net [27]. While 3D convolution architectures are capable of extracting feature representations pertaining to 3D anatomical structures, they also require significantly more parameters compared to their 2D counterparts. Consequently, a number of problems will occur: (1) the deployment and training of 3D models are slow, (2) 3D models consume a lot of GPU memory, which limits the training batch size, (3) the lack of sufficient 3D volume images for training large 3D models leads to overfitting.

**Ultra-high dimension of the 3D volumes.** In contrast to 2D images, 3D volume images have a very high dimension, which makes modeling the 3D volume distribution extremely difficult. In practice, it is infeasible to design a 3D generative model that captures the 3D volume distribution exactly. As a result, approximation techniques such as variational inference or distribution factorization need to be adopted. The resolution of synthesized images is usually limited to small values, such as  $64 \times 64 \times 64$  or  $128 \times 128 \times 128$ , to reduce the data dimension. In contrast, 2D image synthesis can use resolutions of up to  $1024 \times 1024$ .

## 3 3D BRAIN AND HEART APPLICATIONS OF GENERATIVE MODELS

In each of the following subsections, we describe the application background, elaborate on the methods for brain and heart applications, and provide a summary table showing the investigated organ, the model, the datasets, and the performance metrics.

### 3.1 Unconditional Synthesis

The most straightforward application of generative models for 3D medical imaging is unconditional synthesis. By accurately representing the real data distributions of 3D medical volumes, synthesized images of high quality can be produced for downstream tasks such as tumor prediction [44] and Alzheimer’s disease diagnosis [98, 114]. These simulated images can help mitigate two major challenges in data collection: (1) data deficit, which arises from the need for specialized annotation, privacy concerns, and financial constraints, and (2) data imbalance in terms of attributes like health status, age, race, and skin color. Compared to 2D medical imaging, 3D medical imaging places a greater emphasis on the utility of synthesized images. The number of 3D volume images in existing medical datasets ranges from hundreds [18] to thousands [74], which is not enough to train a reliable deep diagnosis model for clinical use. With the rapid development of generative models for natural images, a number of successful architectures have been modified for 3D medical volume

Table 2. Summary of publications on 3D Unconditional Synthesis related to the brain or heart.

Publication (Year)	Organ	Model	Dataset	Metrics
3D- $\alpha$ -WGAN-GP [100] (2019)	Brain	$\alpha$ -GAN [169] WGAN-GP [59]	ADNI [215], BRATS 2018 [9] ATLAS [112]	MMD, MS-SSIM
SlabGAN [56] (2019)	Brain	ProgressiveGAN [86]	fastMRI [241]	FID
Özbey <i>et al.</i> [142] (2020)	Brain	GAN [55]	IXI [36]	PSNR, FID
2D Slice VAE [207] (2020)	Brain	VAE [92]	HCP [201]	RAS, MMD, MS-SSIM
3D StyleGAN [74] (2021)	Brain	StyleGAN2 [88]	ADNI [215], ABIDE [41], HABS [33] OASIS [125], MCIC [53], PPMI [126] ADHD [32], Harvard, GSP [73]	bMMD <sup>2</sup> , MS-SSIM, FID
DCR- $\alpha$ -GAN [174] (2021)	Brain	$\alpha$ -GAN [169]	ADNI [215]	MMD, MS-SSIM, IoU
Shape+Texture GAN [24] (2021)	Brain	WGAN-GP [59]	HCP [201], ADNI [215]	MMD, MS-SSIM
Split&Shuffle-GAN [119] (2022)	Brain Heart	StyleGAN2 [88]	COCA [2], ADNI [215]	FID
HA-GAN [188] (2022)	Brain	GAN [55], AE [67]	Harvard GSP [73]	FID, MMD, IS
DDM [91] (2022)	Heart	DDPM [70]	ACDC [13]	PSNR, NMSE, Dice

synthesis, e.g., VAE [92], Progressive GAN [86], StyleGAN [88],  $\alpha$ -GAN, etc. There are a number of publications that describe unconditional synthesis, as shown in Table 2.

**3.1.1 AE and VAE.** AE and VAE structures are commonly used in medical generative models, either alone or in combination with GANs. Based on a combined two-dimensional slice-level VAE and slice correlation model, 2D Slice VAE [207] generated 3D MRI brain volumes. The VAE was simply trained on MRI brain slices to form a latent space, from which the latent code was sampled for slice generation. To ensure the completeness and consistency of the slices in the generated volumes, the means and covariances of each dimension of the latent code were separately estimated from the training slices. Moreover, [207] proposed a Realistic Atlas Score (RAS) based on the affine-registered segmentations of the generated volumes as an evaluation metric. As a generalization of the VAE model, DDPM [70] was used in DDM [91] for the task of 4-Dimensional (3D+t) temporal cardiac MRI generation. A Diffusion module was trained to estimate the latent code  $c$ , which was then leveraged by the Deformation module to generate deformed images with the spatial transformation layer [82]. 3D- $\alpha$ -WGAN-GP [100] adapted the  $\alpha$ -GAN structure, which combines both the VAE and GAN into a single model to generate 3D brain MRI volumes from random vectors. The architecture consists of a Generator, a Discriminator, an Encoder, and a Code Discriminator. To improve the training stability, the model was trained with the WGAN-GP loss [59] and the reconstruction loss. The integration of VAE and GAN simultaneously addressed the mode collapse and image blurriness problems. Similarly, the  $\alpha$ -GAN structure was also employed in DCR- $\alpha$ -GAN [174], which integrated a Refiner Network with four ResNet blocks after each generator to refine the generation process and produce more realistic images.

**3.1.2 GANs.** In GANs, the progressive growing strategy [86] has been verified to improve the quality and stability of image generation. SlabGAN [56] directly extended the 2D ProgressiveGAN [86] for the 3D generation of MRI brain images. Specifically, SlabGAN replaced the original  $4 \times 4$  constant with  $4 \times 4 \times 4$  to finally generate volumes of  $256 \times 256 \times 16$  resolution. HA-GAN [188] designed a hierarchical generation structure containing two branches: the full volume low-resolution generation branch and the sub-volume high-resolution generation branch. Each branch consists of a GAN network and an AE network with a shared decoder/generator. The two branches also share the low-resolution generation block to facilitate progressive generation. Özbey *et al.* [142] progressively generated 3D volumes with three sequential GAN models. An Axial GAN  $G_A$  generated MRI volumes by concatenating cross-sections [35] in the axial view. Taking the generated volumes as inputs,

a Coronal GAN  $G_C$  was trained to enhance the quality of the coronal view. Similarly, a Sagittal GAN  $G_S$  enhanced the previously generated volumes in the sagittal direction. The Shape+Texture GAN [24] incorporated the geometric deformation technique [106] in two GANs: Shape Network and Texture Network. Shape Network was trained to generate the 3D deformation field from a random vector. To obtain synthetic images, the generated 3D fields were applied to the Montreal Neurological Institute (MNI) brain template to warp it. Both deformed and real images were utilized to train the Texture Network composed of a U-Net [168] and a patch-GAN [109] discriminator.

**3.1.3 StyleGAN.** As a result of the style-based generation technique [87, 88], StyleGAN [87] no longer requires the progressive generation strategy [86]. 3D StyleGAN [74] extended the state-of-the-art 2D StyleGAN2 [88] architecture for 3D medical images generation. Specifically, the mapping network for generating each layer’s style vectors remained unchanged from 2D to 3D. The generator was lifted to 3D with 3D convolution operations and the  $4 \times 4$  constant input was replaced with  $5 \times 6 \times 7$  to fit the 3D brain volumes. The discriminator was also lifted with 3D convolutions. A total of 7,392 image volumes were collected from eight datasets to train the model. The Split&Shuffle-GAN [119] addressed the training challenges of the 3D StyleGAN from the perspective of the training strategy and network architecture. First, a 2D CNN was trained, and then five strategies were proposed to inflate the 2D weights to 3D. The Channel Split&Shuffle modules were respectively devised for the discriminator and the generator to significantly reduce the number of parameters. Both the brain and heart synthetic volume images were generated in [119].

**3.1.4 Quality Assessment.** In evaluating the quality of 3D synthetic volume images, it is important to consider the 3D anatomical structure, which is not evident in a 2D image. As a result, [194] assessed various image quality metrics on MRI images generated by GANs, and proposed a Deep Quality Assessment (QA) model that was trained according to the human ratings of MRI images. Among all, Fréchet Inception Distance (FID) [66], Naturalness Image Quality Evaluator (NIQE) [131], and Maximum Mean Discrepancy (MMD) [15] showed good sensitivity to low-quality images. Deep Quality Assessment managed to distinguish between high-quality images exhibiting subtle variations.

## 3.2 Classification

Table 3. Summary of publications on 3D Classification related to the brain or heart.

Publication (Year)	Organ	Model	Dataset	Metrics
SCGANs [245] (2017)	Heart	GAN [55]	UK Biobank [186]	ACC, Pre, Rec
Biffi <i>et al.</i> [14] (2018)	Heart	VAE [92]	Multi-centre [14], ACDC [13]	ACC
3D-CapsNet [98] (2019)	Brain	AE [67]	ADNI [215]	ACC, ROC
3DPixelCNN [153] (2019)	Brain	PixelCNN [202]	DWI [153], GM [153]	Dice, ACC, MSE
Puyol-Antón <i>et al.</i> [154] (2020)	Heart	VAE [92]	Biobank [186]	Balanced ACC, Sen, Spe

ACC: accuracy. Pre: precision. Rec: recall. Sen: sensitivity. Spe: specificity.

The classification of medical images has a multitude of applications, including Alzheimer’s disease detection [98], cardiovascular diseases diagnosis [14], age/sex prediction [152, 153], etc. For the highest level of accuracy, these applications rely on anatomical structures within the 3D medical volume. To apply deep learning techniques for 3D medical volume classification, 3D CNNs are commonly used [18, 84, 137, 181]. Two problems arise when 3D CNNs are used for 3D volume classification: insufficient training data and lack of explainability. Synthesizing volumes (either



unconditionally or conditionally) to augment the training data can address the issue of insufficient data.

Clinicians are interested not just in the classification outcomes but also in explanations that pinpoint specific regions of the image that support these results [39, 162]. This can be accomplished by interpreting the classifier or learning meaningful latent spaces [154]. Models that offer explanations will enhance trust among clinicians and expedite the transition of deep learning algorithms into practical diagnostic tools in a clinical setting.

A list of generative models for the 3D classification task is shown in Table 3.

SCGANs [245] tackled the problem of classifying missing apical slices (MAS) and missing basal slices (MBS). A Semi-Coupled GANs was designed to include two generators, one for positive and one for negative data generation. A shared discriminator was designed to perform two classification tasks: real/fake and positive/negative. After GANs training, the MAS/MBS classifier was trained on both generated and real data. Puyol-Antón *et al.* [154] performed interpretable Cardiac Resynchronisation Therapy response prediction using a VAE and several classifiers. The volume data was constructed by temporally sampling  $T = 25$  points to extract 2D echocardiography images. VAE processed the slice-level segmentations and concatenated all the  $T$  latent codes. The primary classifier and the multiple concept classifiers used the latent codes for prediction and interpretation, respectively. In order to accurately detect Alzheimer’s disease in its early stages with small-scale datasets, 3D-CapsNet [98] was designed to perform Content-Based Image Retrieval (CBIR). The model consisted of a pre-trained sparse Autoencoder, a 3D Capsule Network [170], and a 3D Convolutional Neural Network [84]. 3DPixelCNN [153] directly extended the PixelCNN [202] model to handle 3D brain MRI volumes. Moreover, by applying SpatialDropout [193], the 3DPixelCNN became a Bayesian model capable of performing uncertainty estimating [50]. The following three semi-supervised tasks were evaluated: semantic segmentation of lesions, age regression, and sex classification. Biffi *et al.* [14] proposed an interpretable model that can be used to automatically classify cardiac diseases caused by structural remodeling, e.g., hypertrophic cardiomyopathy. The segmentation masks from end-diastolic and end-systolic phases were input to a VAE model to learn meaningful latent distributions. Mean vectors of the latent distributions were used to train an MLP classifier. The partial derivative of the class labels w.r.t the mean vector was iteratively updated so as to generate interpretable visualization results.

### 3.3 Conditional Synthesis

In the case of unconditional synthesis, high-quality 3D medical volumes can be generated solely from random input variables. This limits its applications to a broader range of tasks such as class-conditional generation [6, 152], reconstruction [43, 75], and cross-modality synthesis [111, 143, 177, 213, 237, 249]. These tasks can be modeled into the conditional synthesis framework, where extra information can be conditioned for medical volume generation (Fig. 3(b)). Depending on the conditional information, a vector or an imaging modality can be used, resulting in models like Conditional GAN [130] or image-to-image translation [81]. The formulation of the task and the design of the model depend heavily on how the conditional information is incorporated, which will be elaborated below. A list of relevant models for conditional synthesis is provided in Table 4.

**3.3.1 Class / Attribute Condition.** CounterSynth [152] proposed a counterfactual augmentation approach to generate biological-plausible 3D brain volumes conditioned on demographic attributes. Specifically, the U-Net generator is conditioned on the real brain image and counterfactual attributes (e.g., age, sex) to produce the deformation fields, which are then applied to the real brain image to obtain the counterfactual brain image. The discriminator consists of a real/counterfactual classifier and an attribute classifier. By conditioning on label maps instead of vectors, XCAT-GAN [6] can



Table 4. Summary of publications on 3D Conditional Synthesis related to the brain or heart.

Publication (Year)	Organ	Model	Dataset	Metrics
PAN <i>et al.</i> [143] (2018)	Brain	CycleGAN [253]	ADNI [215]	ACC, Sen, Spe, PSNR F1-score, AUC, MCC
3D cGAN [235] (2018)	Brain	cGAN [130]	BRATS [9]	PSNR, NMSE, Dice
Liao <i>et al.</i> [111] (2018)	Heart	GAN [55]	Own [111]	Dice, ASSD
Joyce <i>et al.</i> [85] (2019)	Heart	VAE [92]	ACDC [13]	Dice
Ea-GANs [236] (2019)	Brain	GAN [55]	IXI [36], BRATS [9]	PSNR, NMSE, SSIM
TPSDicyc [208] (2019)	Brain	CycleGAN [253]	IXI [36]	MSE, PSNR, SSIM
Zhang <i>et al.</i> [75] (2020)	Brain	ESRGAN [211]	IXI [36]	PSNR, SSIM
dEa-SA-GAN [237] (2020)	Brain	GAN [55], AE [67]	BRATS [9], SISS2015 [124]	PSNR, NMSE, SSIM
3D-RevGAN [113] (2020)	Brain	RevGAN [200]	ADNI [215]	RMSE, PSNR, SSIM ACC, Sen, Spe, AUC
QSMGAN [20] (2020)	Brain	WGAN-GP [59]	Own [20]	L1, PSNR, NMSW HFEN, SSIM
XCAT-GAN [6] (2020)	Heart	cGAN [130]	ACDC [13], SCD [158], York [7]	DSC, HD
Mcmt-gan [78] (2020)	Brain	GAN [55]	IXI [36], NAMIC [133]	PSNR, SSIM, Dice
CNet [43] (2020)	Heart	U-Net [168]	Own [43]	MSE, SSIM
Lin <i>et al.</i> [114] (2021)	Brain	RevGAN [200]	ADNI [215]	PSNR, SSIM, Accuracy Sen, Spe, AUC
CAE-ACGAN [231] (2021)	Brain	CVAE [183], ACGAN [139]	Own [231]	PSNR, SSIM, MAE
CACR-Net [146] (2021)	Brain	GAN [55]	BRATS [9]	NMSE, SSIM, PSNR
DiCyc [209] (2021)	Brain	CycleGAN [253]	IXI [36]	MSE, PSNR, SSIM
ProvoGAN [240] (2022)	Brain	GAN [55]	In vivo Brain [240], IXI [36]	PSNR, SSIM
ResViT [34] (2022)	Brain	AE [67]	IXI [36], BRATS [9]	PSNR, SSIM
Subramaniam <i>et al.</i> [185] (2022)	Brain	WGAN [59]	PEGASUS [134], 1000Plus [76]	FID, PRD, DSC, bAVD
CounterSynth [152] (2022)	Brain	StarGAN [23]	UK Biobank [186]	ACC, MAE, FID
HDL [220] (2022)	Heart	Pixel-to-pixel [81]	3Dir MVM [180]	MSE, PSNR, SSIM
Qiao <i>et al.</i> [156] (2022)	Heart	CycleGAN [253]	UK Biobank [186]	DICE, HD, ASSD

Own: The dataset was originally collected and processed by the authors of the paper.

ACC: accuracy. Sen: sensitivity. Spe: specificity. PRD: precision and recall of distributions.

bAVD: balanced average Hausdorff distance. DSC: dice similarity coefficient.

ASSD: average symmetric surface distance. MCC: Matthews correlation coefficient

synthesize high-fidelity cardiac MRI images. First, a U-Net [168] was trained to obtain the 4-class or 8-class segmentation masks. The real images and masks were then fed as inputs to conditional GANs for image synthesis. The downstream cardiac cavity segmentation task was used to evaluate the generated data after the GANs training. In order to produce 3D cardiac synthetic MRI images, Joyce *et al.* [85] conditioned the synthesis on a learned anatomical model. The samples from the anatomical model and random Gaussian noises were input to the sequential transform and render modules to generate synthetic volumes. All the model parameters were trained through self-supervision with a reconstruction error. Xia *et al.* [218] conditioned on difference age vectors to synthesize age-progressed 2D slices, which had the potential for 3D volumes. Qiao *et al.* [156] considered both age and gender in a conditional generative model to generate 3D anatomy of the ageing heart. The model consisting of a cycle-consistent reconstruction and a self-reconstruction module was applied to cross-sectional and longitudinal datasets.

**3.3.2 Cross-modality Synthesis.** Among the early works, 3D cGAN [235] extended the 2D image-to-image translation GANs model [81] to synthesize the 3D FLuid-Attenuated Inversion Recovery (FLAIR) from 3D T1 MRI images. Local adaptive fusion was applied to improve the FLAIR details. dEa-SA-GAN [237] proposed sample adaptive GAN models to explore both the global space mapping and the local space mapping. The whole model consists of two paths. The baseline path is a standard 3D GAN used to learn global mapping. The sample-adaptive path

uses the neighborhood relationships between the training samples to force local sample-specific learning. Two synthesis tasks were conducted in dEa-SA-GAN:  $T1 \rightarrow \text{FLAIR}$  and  $T1 \rightarrow T2$ . CACR-Net [146] designed a confidence-guided aggregation and cross-modality refinement network for the multi-modality MRI synthesis task. The Confidence-Guided Aggregation Module uses two U-Net generators to process two different input modalities. The two outputs are then aggregated and input to the Cross-Modality Refinement Module for further improvement. Three synthesis tasks were conducted:  $T1+T2 \rightarrow \text{FLAIR}$ ,  $T1+\text{FLAIR} \rightarrow T2$ , and  $T2+\text{FLAIR} \rightarrow T1$ . For CAE-ACGAN [231], only a single CT image was used to generate multi-contrast MRI images (i.e., fat, R2, and water). The Conditional Variational AutoEncoder (CVAE) [183] and ACGAN [139] architectures were developed to take advantage of the capabilities of both VAE and GAN. The structure of CAE-ACGAN consists of an Encoder, a Generator, a Discriminator, and a Classifier. Mcmt-gan [78] proposed an unsupervised modality transferable framework for 3D brain image synthesis. To ensure robust and high-fidelity cross-modal generation, Mcmt-gan introduced three losses (i.e., cycle-consistency loss, bidirectional adversarial loss, and domain adapted loss) and a volumetric manifold regularization. Moreover, a fault-aware discriminator was proposed to make the model coherent with the segmentation task. The cross-modality synthesis tasks include: Proton Density (PD) $\rightarrow T2$ ,  $T2 \rightarrow \text{PD}$ ,  $T1 \rightarrow T2$ , and  $T2 \rightarrow T1$ . To reflect the texture details of image structure, Ea-GANs [236] devised an edge-aware generative adversarial network for cross-modality synthesis. Specifically, the edge information was extracted by the Sobel [51] edge detector and incorporated in the training process of GANs. Two variants were proposed depending on where the edge information was included in the objective function: gEa-GAN (generator) and dEa-GAN (generator and discriminator). Both the  $T1 \rightarrow \text{FLAIR}$  and  $T1 \rightarrow T2$  tasks were evaluated. Recently, the Transformer [203] was adopted in ResViT [34] for the first time to conduct multi-modality synthesis. The generator of ResViT has an encoder-decoder structure with multiple Aggregated Residual Transformer (ART) blocks between the encoder and the decoder. The weight-shared ART blocks are able to distill the task-specific information, such as location and context. Three synthesis tasks were conducted:  $T1, T2 \rightarrow \text{PD}$ ,  $T1, T2 \rightarrow \text{FLAIR}$ , and  $\text{MRI} \rightarrow \text{CT}$ . To tackle the issue of domain-specific deformations in cross-domain synthesis, DiCyc [209] incorporated deformable convolution layer in CycleGAN and designed additional two losses: domain-invariant cycle consistency loss and NMI-based alignment loss. The synthesis tasks were:  $T2 \rightarrow \text{PD}$ ,  $\text{PD} \rightarrow T2$ ,  $\text{CT} \rightarrow T2$ , and  $T2 \rightarrow \text{CT}$ . To tackle the misalignment between the source domain and synthesized images, TPSDicyc [208] improved DiCyc with a Spatial Transformation Network (STN) to model the relative deformation. The  $\text{PD} \rightarrow T2$  and  $T2 \rightarrow \text{PD}$  synthesis were evaluated on brain MR images.

By using cross-modality synthesis, volumetric data for a specific modality can be completed. Liao *et al.* [111] introduced a cross-modality volume completion task to assist in the segmentation of IntraCardiac Echocardiography images. A GAN model named 3D segmentation and completion network (3D-SCNet) was proposed in [111] to perform simultaneous completion and segmentation. A number of cross-modality completion methods have been proposed to improve Alzheimer's disease diagnosis [114, 143, 200]. PAN *et al.* [143] utilized the CycleGAN [253] model to perform 3D PET image imputation from MRI and likely incomplete PET images. Then, the imputed PET and MRI were used by the Landmark-based Multi-Modal Multi-Instance Learning (LM<sup>3</sup>IL) for Alzheimer's disease classification. In 3D-RevGAN [113] and Lin *et al.* [114], the 3D Reversible GAN [200] was adopted to complete the missing PET data for Alzheimer's Disease diagnosis. Specifically, Lin *et al.* [114] proposed a two-step method: (1) learn the bidirectional mapping between PET and MRI images with a 3D Reversible GAN, and (2) train a 3D CNN to classify the disease. Reversible GAN has the advantage of only using one generator instead of two in CycleGAN.

There are some other tasks that are related to the cross-modality/multi-modality synthesis, e.g., quantitative susceptibility mapping (QSM) [20] and Time-of-Flight Magnetic Resonance Angiography (TOF-MRA) generation [26, 185]. An architecture based on the 3D U-Net was used by

QSMGAN [20] to synthesize QSM. WGAN with gradient penalty was used to improve the training stability. Subramaniam *et al.* [185] simultaneously generated the TOF-MRA patches along with the corresponding brain vessel segmentation labels. To improve efficiency, four variants of the WGAN architecture were considered and the mixed precision technique was applied. For the cardiac digital twins task, HDL [220] proposed a hybrid deep-learning framework consisting of a hybrid UNet for temporal interpolation, a GAN for phase synthesis and a velocity assessment module. For phase synthesis, magnitude images were input to the pixel-to-pixel [81] model to synthesize phase images. For COVID-19 CT images, a controllable and simultaneous synthesizer (CS<sup>2</sup>) was proposed in [221] to generate both images and corresponding segmentation masks for data augmentation.

**3.3.3 Reconstruction/Recovery.** A complex-valued CNN (i.e., CNet [43]) was used to reconstruct under-sampled 3D Late Gadolinium Enhancement (LGE) cardiac MRI data. The overall architecture adopted a U-Net structure with several complex-valued components: complex convolutional layer, radial Batch Normalization (BN) layer, down-sampling and up-sampling layers, and complex activation function. CNet achieved better performance compared to real-valued networks and faster speed compared to compressed sensing. Zhang *et al.* [75] used a 2D super-resolution technique to perform 3D Brain MRI super-resolution reconstruction. A super-resolution GAN (i.e., ESRGAN [211]) was applied to 2D brain slices, followed by a Bilinear interpolation to complete the null values. ProvoGAN [240] proposed a progressively volumetric strategy to decompose the 3D volume recovery into sequential 2D cross-sectional mappings. The three rectilinear orientations (axial, coronal, sagittal) were gradually processed in the first, second, and third progression steps. In each step, a 2D GAN was trained based on the previous step results. ProGAN outperformed both volumetric and cross-sectional models on the MRI recovery and synthesis tasks.

## 3.4 Segmentation

Image segmentation is one of the most important medical imaging applications. It can be utilized to either assign corresponding labels to different anatomical structures (e.g., different cardiac chambers) or highlight specific regions of interest (e.g., brain tumor or lesion areas). Automatic segmentation liberates medical experts from the time-consuming and tedious task of manually annotating the anatomical structures/disease regions. 3D volume segmentation offers more detail and anatomical information than 2D image segmentation, which is the focus of this subsection. This subsection is organized according to different segmented structures/regions of interest in the brain and heart. Hopefully, this will assist researchers in finding their target models more quickly. Table 5 provides a list of the most relevant methods.

### 3.4.1 Brain.

**Tumor segmentation.** Brain tumor segmentation has gained great research interest recently [122], especially for 3D brain volumes [19, 28, 135, 147, 165, 196, 239, 242]. Myronenko [135] used an encoder-decoder structure for tumor subregion segmentation, which consists of a shared encoder, a segmentation decoder and a reconstruction VAE decoder. S3D-UNet [19] proposed a separable U-Net architecture that replaces the original 3D convolution with a three-branch separable 3D convolution for brain tumor segmentation. Peng *et al.* [147] proposed a multi-scale 3D U-Net architecture to capture the features from different spatial resolutions. The architecture consists of several 3D U-Net blocks, with each block utilizing a 3D separable convolution instead of a standard convolution to reduce the time and memory complexities. Vox2Vox [28] devised a 3D volume-to-volume GAN to segment brain tumors, composed of a U-Net generator to transform images to masks and a PatchGAN [109] discriminator for adversarial learning. Zhang *et al.* [242] proposed a cross-modality framework based on CycleGAN [253] to segment brain tumors from multi-modality

Table 5. Summary of publications on 3D Segmentation related to the brain or heart.

Publication (Year)	Organ	Model	Dataset	Metrics
Salehi <i>et al.</i> [171] (2017)	Brain	U-Net [168]	MSSEG [31]	DSC, Sen, Spe, F2, APR
Myronenko [135] (2018)	Brain	VAE [92]	BRATS [9]	Dice, HSD
S3D-UNet [19] (2018)	Brain	U-Net [168]	BraTS [9]	Dice, Sen, Spe, HD95
voxel-GAN [165] (2018)	Brain	cGAN [130], U-Net [168]	BRATS [9], ISLES [124]	Dice, HSD, Spe, Sen
Mondal <i>et al.</i> [132] (2018)	Brain	U-Net [168], GAN [55]	iSeg-2017 [80], MRBrainS [127]	DSC, ASD
Yang <i>et al.</i> [230] (2018)	Heart	GAN [55], U-Net [168]	Own [230]	PSNR, MSE
MuTGAN [227] (2018)	Heart	GAN [55]	Own [227]	ACC, Dice, Sen Spec, Infarct Size, etc.
VoxelAtlasGAN [42] (2018)	Heart	cGAN [130]	Own [42]	MSD, HSD, Dice, Corr of EF
Zhang <i>et al.</i> [247] (2018)	Heart	CycleGAN [253]	Own [247]	Dice, S-score
Liu <i>et al.</i> [115] (2019)	Brain	GAN [55], U-Net [168]	BRATS [9]	Dice
RP-Net [210] (2019)	Brain	U-Net [168]	CANDI [72], IBSR [167]	DSC
DSTGAN [226] (2020)	Heart	GAN [55]	Own [226]	ACC, Dice, Infarct size IoU, Per-size, Per-seg
PSCGAN [228] (2020)	Heart	GAN [55]	Own [228]	SSIM, NRMSE, PSNR, Dice ACC, Sec, Spe
Yuan <i>et al.</i> [239] (2020)	Brain	GAN [55]	Decathlon [178]	Dice, RAVD, ASSD, MSSD HD95, Sen, Spe
3D DR-UNet [204] (2020)	Heart	U-Net [168]	ACDC [13], LASC [138]	DSC, HD, ASD
Peng <i>et al.</i> [147] (2020)	Brain	U-Net [168]	BraTS [9]	Dice
SASSNet [110] (2020)	Heart	GAN [55]	Left Atrium [225]	Dice, Jaccard, ASD, HD95
Vox2Vox [28] (2020)	Brain	Pixel-to-pixel [81] U-Net [168]	BRATS [9]	Dice, HD95
Kolarik <i>et al.</i> [94] (2021)	Brain	U-Net [168]	MSSEG [31]	Dice, Sen
FM-Pre-ResNet [60] (2021)	Heart	VAE [92], U-Net [168]	MM-WHS [256]	DSC, Jaccard, SD, HD
Ullah <i>et al.</i> [196] (2021)	Brain	U-Net [168]	BRATS [9]	Dice
MVSGAN [155] (2021)	Heart	GAN [55]	Own [155], STACOM2011 [187]	Dice, Jaccard, HD
Zhang <i>et al.</i> [242] (2021)	Brain	CycleGAN [253], U-Net [168]	BRATS [9]	Dice, HD95, Sen
DAR-UNet [233] (2022)	Brain	GAN [55], U-Net [168]	Vestibular Schwannoma [175]	Dice, ASD
Bustamante <i>et al.</i> [17] (2022)	Heart	U-Net [168]	Own [17]	Dice, HD, ASD, Sen Precision, miss rate
Xing <i>et al.</i> [223] (2022)	Heart	U-Net [168]	Own [179]	MAE, PSNR, SSIM

Own: The dataset was originally collected and processed by the authors of the paper.

ACC: accuracy. Sen: sensitivity. Spe: specificity. PPV: positive predictive value. HD95: 95% Hausdorff distance.

DSC: dice similarity coefficient. MSD: mean surface distance. HSD: Hausdorff surface distance.

ASD: average surface distance. EF: ejection fractions. Per-size: percentage of infarct size, Per-seg: percentage of segments.

brain data. Specifically, two sub-modules were designed: a CycleGAN-based Cross-modality Feature Transition module to perform cross-modality synthesis, and a Cross-modality Feature Fusion module to integrate multi-modality features for tumor segmentation. The conditional GAN model was used in voxel-GAN [165] to address the imbalanced tumor segmentation task. In order to deal with the imbalance issue, a cGAN that contained a segmentor and discriminator was designed with a weighted adversarial loss. Yuan *et al.* [239] conducted multi-modal segmentation with only unpaired 3D medical volumes. The segmentation task and auxiliary cross-modality translation tasks were tackled in a unified framework, consisting of modules for modality translation and modality recovery. Each module contained a shared encoder, a segmentation decoder, and a translation decoder. Ullah *et al.* [196] evaluated a number of MRI image pre-processing techniques for improving and segmenting MRI images. Gibbs ringing artifact removal was found to be the best processing technique.

**Sclerosis lesion segmentation.** To address the data imbalance problem of segmenting sclerosis lesions, Salehi *et al.* [171] used the U-Net structure and proposed a new generalized loss function called Tversky loss. For better imbalanced segmentation, the Tversky loss used both the Dice

similarity coefficient (DSC) and  $F_1$  score. Kolarik *et al.* [94] proposed a transfer learning framework for lesion segmentation in which pre-trained 2D CNN weights were transferred to 3D networks. Specifically, a Planar 3D U-Net was proposed based on the 3D Planar convolution to conduct lesion segmentation. For 2D center axial slice, Basaran *et al.* [12] proposed a foreground-based generative model to synthesize pseudo-healthy images and lesions for downstream segmentation tasks.

**Brain tissue segmentation.** RP-Net [210] segmented the brain tissues into three classes: cerebrospinal fluid (CSF), gray matter (GM), and white matter (WM). RP-Net modified the U-Net structure in [168] and introduced both a pyramid pooling module and a recursive residual module. Then, multiple stacks of deep networks were constructed with these modules. Mondal *et al.* [132] performed the 3D multi-modal brain tissue segmentation task in a few-shot setting where only few labeled data were provided. Specifically, the labeled volumes were input to a U-Net generator to predict the segmentation masks, while the unlabeled volumes underwent a variational autoencoder to perform the reconstruction task.

**Others.** Four MRI sequences (T1, T1c, T2, FLAIR) were used by Liu *et al.* [115] to segment glioma subregions into three classes: whole tumor (WT), enhancing tumor (ET) and tumor core (TC). Specifically, they proposed a GAN-regularized 3D U-Net structure, which uses a pixel-to-pixel scheme to concatenate the input with labels for effective training. DAR-UNet [233] modeled the cross-modality medical image segmentation (e.g., brain structure segmentation) within an Unsupervised Domain Adaptation (UDA) framework. The first step was to train multiple GANs to disentangle the style and content of both the source and target images. Then, these styles were used to generate diverse target images, which were used to train the segmentation model.

### 3.4.2 Heart.

**Whole heart structure segmentation.** FM-Pre-ResNet [60] proposed two novel designs for segmenting the whole heart structure. First, the feature merge residual unit was designed to improve existing pre-activation residual units. Second, 3D VAE was used to perform the volume reconstruction task, which regularized and assisted the segmentation task. Zhang *et al.* [247] proposed a cross-modality synthesis approach with unpaired training data to boost the multi-modal volume segmentation performance. For the cross-modality synthesis task, two GANs were used to construct the CycleGAN [253], and the segmentation task utilized the synthesized data to augment the training data. The model was trained with cycle-consistency loss, adversarial loss, and shape-consistency loss. Heart segmentation was accomplished using a multi-stage procedure in 3D DR-UNet [204]: a low-resolution localized map was first generated with a Localization Network, then the high-resolution volume was cropped based on the map and fed into a Segmentation Network to finally generate the segmentation mask. Both the Localization Network and the Segmentation Network were built using the 3D Dilated Residual U-Net architecture. For the automatic segmentation of the 4D flow MRI volume, Bustamante *et al.* [17] used the U-Net structure instead of the regular 3D volume segmentation. With the proposed method, the four cardiac chambers, the aorta, and pulmonary artery were all segmented.

**Left ventricle (LV) / left atrium (LA) segmentation.** VoxelAtlasGAN [42] addressed the 3D LV segmentation task on echocardiography images. A new voxel-to-voxel mode of the conditional GANs was devised to include the 3D LV atlas as powerful condition information, addressing issues with limited annotation and low contrast in echocardiography. In addition, a consistent constraint was proposed to enhance the discrimination loss. Yang *et al.* [230] proposed a probability-based method to segment the LV myocardium, avoiding the boundary-moving issues associated with threshold-based methods. A 3D U-Net generator was used to propagate the partial 2D slice



segmentation to the whole 3D volume, and a 3D CNN discriminator was used to distinguish the ground truth and the generated segmentation masks. MVSGAN [155] tackled the short-axis (SAX) view segmentation of 3D cardiac MRI volumes, which was hampered by the sparse spatial structure. Three modules were devised in MVSGAN: (1) a residual adversarial fusion (RAF) module to examine the inter-slice dependency and anatomical priors, (2) a structural perception-aggregation (SPA) module to model the correspondence between segmentation labels and cardiac models, and (3) a joint training objective for multi-task learning. SASSNet [110] proposed a shape-aware method for semi-supervised 3D LA segmentation [238], incorporating geometric shape constraints into the GANs framework. More specifically, the adversarial generation of Signed Distance Map (SDM) serves as an auxiliary task to augment the LA segmentation. The shared segmentation network (generator) adopts a V-Net [129] to simultaneously generate the SDM and segmentation mask. Xing *et al.* [223] proposed a multi-task attention structure utilizing three UNets to synthesize three-directional CINE multi-slice myocardial velocity mapping (3Dir MVM) and the corresponding left ventricle segmentation.

**Myocardial infarction (MI) segmentation.** A generative and multi-task learning framework was proposed in MuTGAN [227] for simultaneous quantification and segmentation of myocardial infarction (MI). Specifically, the MuTGAN generator consists of two networks: a spatial-temporal feature extraction network (SFEN) to extract the comprehensive spatio-temporal correlations and a joint feature learning network to learn the interaction between segmentation and quantification. The discriminator consists of a task-relatedness network to learn the intrinsic task patterns. DSTGAN [226] extended MuTGAN [227] with several enhancements: a new feature learning network (spatio-temporal variation encoder), a conditional GAN, and three iterative task-specific discriminators.

**Ischemic disease image segmentation.** PSCGAN [228] proposed the first one-stop contrast agent-free framework to simultaneously synthesize and segment the Ischemic Heart Disease (IHD) related cine MR images. The proposed framework is a progressive model integrating three consecutive GAN phases: prior generation, conditional synthesis, and fine segmentation. Each phase uses a similar sequential causal learning framework with two pathways: a spatial perceptual pathway and a temporal perceptual pathway. A synthetic regularization loss and a segmentation auxiliary loss were specially designed to facilitate the model training.

### 3.5 Denoising

Table 6. Summary of publications on 3D Denoising related to the brain or heart

Publication (Year)	Organ	Model	Dataset	Metrics
Wolterink <i>et al.</i> [216] (2017)	Heart	GAN [55]	Harder <i>et al.</i> [37]	PSNR
LA-GANs [214] (2018)	Brain	GAN [55]	MCI [213]	PSNR, SSIM
3D c-GANs [213] (2018)	Brain	cGAN [130]	MCI [213]	PSNR, NMSE, SUV differences
RED-WGAN [161] (2019)	Brain	WGAN [59]	IXI [36]	PSNR, RMSE, SSIM, IFC
SGSGAN [252] (2022)	Brain	StyleGAN [87]	Own [252]	PSNR, SSIM, MAE, U-Net score

Own: The dataset was originally collected and processed by the authors of the paper.

IFC: information fidelity criterion.

Artifacts and noise may affect medical images collected in practical clinical settings due to factors such as radiation dose, time constraints, and patient discomfort. The purpose of image denoising is to reduce the amount of noise in the original image (e.g., low-dose CT) and recover a high-quality

medical image (e.g., full-dose CT). Denoising Autoencoders and GANs can naturally be applied for image denoising. A list of relevant 3D denoising models is provided in Table 6.

In an early study, Wolterink *et al.* [216] proposed the use of GANs in low-dose CT for noise reduction. A generator network generated routine-dose CT images from low-dose CT images. A discriminator was used to differentiate between the real and generated routine-dose CT images. The GANs were trained using a voxelwise loss. An encoder-decoder and WGAN technique were used to denoise MRI images in RED-WGAN [161]. The residual autoencoder structure was devised for the generator network, while three losses were proposed to train the whole network: adversarial loss, MSE loss, and perceptual loss. 3D c-GANs [213] achieved high-quality (full-dose) PET image synthesis from low-dose CT images using 3D conditional GANs. The 3D U-Net was used as a generator, and a concatenated progressive refinement strategy was proposed. SGSGAN [252] synthesized full-dose PET images using StyleGAN [87] and a segmentation U-Net. Specifically, a style-based generator converted low-dose PET images to full-dose images, which were then processed by the segmentation network and the discriminator network. Based on low-dose PETs and corresponding MRI images, LA-GANs [214] synthesized full-dose PETs. First, a local adaptive fusion module was designed to integrate all input modalities into a fused image. Then, a U-Net generator and a discriminator were adversarially trained with the real/fake full-dose PET images.

### 3.6 Detection

Table 7. Summary of publications on 3D Detection related to the brain or heart

Publication (Year)	Organ	Model	Dataset	Metrics
Uzunova <i>et al.</i> [197] (2019)	Brain	CVAE [183]	BRATS [9], LPBA40 [176]	Dice, Sen, Spec, AUC Jaccard
MADGAN [61] (2021)	Brain	GAN [55]	OASIS-3 [101], Own [61]	AUC
3D MTGA [224] (2022)	Heart	U-Net [168], cGAN [130]	Own [224]	Sen, Spe, Pre, ACC SSIM, PSNR, MAE, RMSE DSC, USR, OSR, Jaccard
Pinaya <i>et al.</i> [151] (2022)	Brain	VQ-VAE [199] Autoregressive Transformer [47]	MedNIST [232], BRATS [9] WMH [99], MSLUB [108] UK Biobank [186]	Dice, AUPRC, AUROC FPR80, FPR95, FPR99

Own: the dataset was originally collected and processed by the authors of the paper.

Sen: sensitivity. Spe: specificity. Prec: precision. ACC: accuracy. FPR: false-positive rates.

DSC: dice similarity coefficient. USR: under-segmentation rate. OSR: over-segmentation rate.

In medical imaging, detection usually refers to the detection of anomalies or pathologies, such as lesions or tumors. A supervised detection method requires large amounts of healthy and anomalous data to effectively differentiate between them. This is often not feasible especially due to the scarcity of anomalous data and data imbalance. Therefore, unsupervised detection methods have been proposed in order to use generative models to capture healthy data distribution. A list of relevant 3D detection models is provided in Table 7 for the brain or the heart.

MADGAN [61] designed a two-step GAN-based medical anomaly detection method to detect different types of brain anomalies at various stages, e.g., Alzheimer’s disease at early and late stages, as well as brain metastasis. The generator uses three consecutive brain MRI slices to generate the next three brain slices, while the discriminator classifies these real/fake next three brain slices. After training, the reconstruction loss (i.e.,  $L_2$ ) between the real and reconstructed three slices is computed to detect anomalies. A multi-task generative framework was proposed in [224] to detect aortic dissection using non-contrast-enhanced CT (NCE-CT) volumes. The framework consists of a 3D nnU-Net to perform aortas segmentation of NCE-CT volumes and a 3D Multi-Task Generative Architecture (MTGA) to perform CE-CT synthesis, true & false lumen segmentation, and



simultaneous aortic dissection detection. Uzunova *et al.* [197] performed unsupervised pathology detection with a 3D CVAE structure. The pathologies were detected by the differences to the learned norm of the healthy image volumes through CVAE reconstruction. Pinaya *et al.* [151] applied a Transformer-based model for unsupervised 3D brain anomaly detection and segmentation when a limited amount of data is required. Specifically, a codebook of brain image representations is learned with the VQVAE [199] architecture. Then, an Autoregressive Transformer uses the codebook to generate brain volumes in a similar way to PixelRNN [202]. Anomalies are considered for Autoregressive Transformer output probabilities lower than a threshold.

### 3.7 Registration

Table 8. Summary of publications on 3D Registration related to the brain or heart

Publication (Year)	Organ	Model	Dataset	Metrics
VTN [250] (2019)	Brain	U-Net [168]	ADNI [215], ABIDE [41], ADHD [32]	Seg. IoU, Lm. Dist., Time
VoxelMorph [11] (2019)	Brain	U-Net [168]	OASIS [125], ABIDE [41], ADHD [32] MCIC [53], PPMI [126], Harvard GSP [73] HABS [33], FreeSurfer Buckner40 [49]	Dice, Jacobian matrix
Deform-GAN [246] (2020)	Brain	GAN [55]	BRATS [9]	RMSE, Dice
Zhu <i>et al.</i> [255] (2021)	Brain	U-Net [168]	Mindboggle101 [93], LPBA40 [176], IXI [36]	DSC, HD, ASSD
Krebs <i>et al.</i> [96] (2021)	Heart	VAE [92]	Own, ACDC [13]	Dice, HD
Ramon <i>et al.</i> [160] (2022)	Brain	GAN [55]	ADNI [215], NIREP [25]	DSC
TGAN [254] (2022)	Brain	GAN [55] U-Net [168]	BrainWeb [29], Atlas [112], RIRE [166]	Dice, mean SSIM

Own: The dataset was originally collected and processed by the authors of the paper.

DSC: dice similarity coefficient. HD: Hausdorff distance. ASSD: average symmetric surface distance.

The purpose of image registration is to find the spatial correspondence (e.g., affine matrix, deformation field) between an image pair. As a result of this correspondence, geometric models like Spatial Transformer Network (STN) [82] can be used to warp the image. Since manually annotating the corresponding points of image pairs is prohibitively laborious, various unsupervised registration approaches based on generative models (e.g., U-Net [168] or GAN [55]) have been proposed. Table 8 lists some of the most relevant 3D registration methods.

VTN [250] proposed an unsupervised Volume Tweening Network (VTN) for 3D volume registration. VTN was constructed by an end-to-end cascade of registration subnetworks to generate deformation fields between images. The registration subnetwork was implemented with either an affine registration subnetwork or a dense deformable registration subnetwork. An invertibility loss was further incorporated to ensure backward consistency. In an end-to-end framework, Zhu *et al.* [255] performed a joint affine alignment and deformable registration. The framework contained an affine alignment subnetwork to learn the affine matrix and a deformable registration subnetwork to generate the deformation fields. An STN [82] was used to warp the volume. The VoxelMorph algorithm [10, 11] formulated registration as a mapping between image pairs and deformation fields. A U-Net processes the input pair to get a registration field, which is then used by STN to warp the image. Both the original image volumes and the segmentation masks could be adopted to train the model. Deform-GAN [246] incorporated mono-modal registration and multi-modal registration in an adversarial framework, which consists of a U-Net-like Transformation Network and Generator, as well as a Discriminator. The registration model was trained using both a GAN loss and a new local gradient loss. Ramon *et al.* [160] combined a GAN with the traditional LDDMM [65] approach and proposed two model variants for the stationary and non-stationary parameterizations. TGAN [254] proposed a two-stage GAN framework for multi-modal brain registration. The GAN of the first stage extracted the structural representation of the registered image, while the

GAN of the second stage estimated the image intensities after registration. For spatial-temporal registration of cardiac cine-MRI sequences, Krebs *et al.* [96] proposed a conditional VAE model based on multivariate Gaussian prior and captured the intrinsic motion into a low-dimensional space (i.e., motion matrix). Motion matrix can be used for temporal interpolation, motion transport, motion simulation, and diffeomorphic tracking.

## 4 DISCUSSION AND FUTURE DIRECTIONS

We have surveyed seven medical applications pertaining to 3D generative models for the brain and heart (from Jan 2017 to Oct 2022): unconditional synthesis, classification, conditional synthesis, segmentation, denoising, detection, and registration. Among them, segmentation and conditional synthesis have the largest number of publications: 25 and 19, showing the great research interest and importance of these two applications. U-Net [168] is the most popular model for segmentation, either used individually or as a generator/encoder network. Image-to-image translation [81, 253] is naturally compatible with conditional synthesis, and is based on models such as cGAN [130], CycleGAN [253], StarGAN [23], etc. Unconditional synthesis covers 10 papers, favoring WGAN-GP [59], VAE [92], and StyleGAN2 [88] models. In the literature, there are only 6 papers on registration, 5 on denoising, and 4 on detection. They are mainly based on the vanilla GAN [55] and U-Net [168] models. The architecture and model design should consider the application requirements, e.g., CycleGAN [253] was widely-used for unsupervised learning [143, 242, 247], and VAE [92] was adopted for interpreting the classification results [14, 154]. As well as models, we also find that metrics and datasets are usually specific to organs and applications, e.g., ADNI [215] dataset for brain applications, Dice metric for segmentation-related tasks.

Although many publications show the effectiveness and application prospects of 3D generative models for medical volumes, this field is still rapidly growing and embraces various potential future directions and techniques. The following are five possible future directions.

### 4.1 Few-shot Learning

Few-shot learning [212] aims to leverage few available examples to effectively train a deep model. It has been extensively researched in computer vision [120] and natural language processing [77]. For example, few-shot image generation [140], few-shot unsupervised image-to-image translation [116] have been investigated for natural images. As a result of the collection procedure, patient consent, and annotation cost, medical applications usually lack sufficient training data. Thus, few-shot learning is naturally suited to medical applications of 3D generative models. Using few training samples, Mondal *et al.* [132] achieved comparable segmentation results for 3D multi-modal volumes, showing promising prospects for 3D medical applications utilizing few-shot learning methods.

### 4.2 Self-supervised Learning

Self-supervised learning (SSL) [118] explores the structural and contextual information lying in the data to provide supervision signals for model training. Self-supervised learning has the advantage of not requiring manual annotations, saving time and money. According to a recent study [62], self-supervised learning can be as effective as or even superior to supervised learning in various computer vision tasks. For 3D medical applications, the utilization of self-supervised learning will mitigate the burden of tedious and laborious annotation, while still achieving satisfactory performance. Joyce *et al.* [85] trained a 3D cardiac MRI synthesis model with only unlabelled data through self-supervision (reconstruction error). Cheng *et al.* [141] showed that 2D few-shot medical segmentation could be realized with self-supervised learning techniques. In the future, we expect more studies to leverage the intrinsic 3D structure of medical volumes as a powerful tool for self-supervised learning.

### 4.3 Efficient 3D Network Architecture

3D network architecture is another bottleneck for effective 3D generative medical applications, in addition to data scarcity. The majority of 3D models for medical volume generation use 3D convolution directly, which is slow and parameter-inefficient. Due to this, existing methods have a small model capacity (e.g., 64 convolution channels [74] and a small synthesized resolution (e.g.,  $64 \times 64 \times 64$  [100])). The development of efficient network architectures for 3D generative models is an important and practical research area. By using Split&Shuffle modules in GANs, [119] reduced over half of the model parameters, and yet achieved better performance on both heart and brain datasets. A comprehensive analysis of resource-efficient 3D CNNs was conducted in [95]. Additionally, neural architecture search (NAS) [45] is a promising direction for designing efficient 3D architectures.

### 4.4 Denoising Diffusion Probabilistic Model (DDPM)

Recent research has shown that DDPMs outperform GANs at generating natural images [40, 71]. DDPM models a Markov chain process to convert the simple Gaussian noise into a real data distribution. When compared to GANs, it can better cover the overall data distribution and have a stationary training objective. As a result, medical applications can also benefit from the DDPM for effective image generation. DDPM [70] was directly used in [150] for unsupervised brain anomaly detection on 2D CT and MRI images. In [91], DDPM was used to estimate the latent code for 4D cardiac MR image generation. We believe that future 3D medical volume models can use DDPM as a good alternative to GANs and VAEs.

### 4.5 Trustworthy, Explainability, and Potential Bias

The pursuit of trustworthy and explainable Artificial Intelligence (AI) is a growing area of research, especially in the field of medical image generation, where diagnostic errors can have severe consequences for patients [162]. Recent research has explored creating reliable and explainable AI solutions for both non-imaging medical data synthesis [222] and medical image analysis [39]. Given that medical datasets often come from various hospitals, each using different scanning equipment and protocols, models trained on a single dataset can exhibit inherent biases and may not be universally applicable. Recent initiatives [136, 222] have tackled this issue by harmonizing and fusing data across multiple modalities and centers to minimize bias and enhance explainability. Additional biases may arise from cultural and geographical factors in data collection and model architecture choices. In this survey, we focus primarily on brain and heart applications when exploring possible 3D volume generation models. We anticipate future research will broaden the scope to include more diverse and explainable medical image-generation techniques.

## 5 CONCLUSION

This paper reviews three types of generative models and their applications to synthetic 3D medical volume generation. A new taxonomy of unconditional and conditional generative models is proposed to cover seven medical applications: unconditional synthesis, classification, conditional synthesis, segmentation, denoising, detection, and registration. We have provided a corresponding table with the organ, model, dataset, and evaluation metrics for each application to make it easier for researchers to locate their model of interest. Finally, with the hope of further progressing future research in this field, four prospective directions are discussed.

## REFERENCES

- [1] Aya Saleh Ahmed, Wessam H El-Behaidy, and Aliaa AA Youssif. 2021. Medical image denoising system based on stacked convolutional autoencoder for enhancing 2-dimensional gel electrophoresis noise reduction. *Biomedical*

*Signal Processing and Control* 69 (2021), 102842.

- [2] Stanford AIMI. 2022. *COCA - Coronary Calcium and chest CT's dataset*. <https://stanfordaimi.azurewebsites.net/datasets/e8ca74dc-8dd4-4340-815a-60b41f6cb2aa>
- [3] Zeynettin Akkus, Alfiya Galimzianova, Assaf Hoogi, Daniel L Rubin, and Bradley J Erickson. 2017. Deep learning for brain MRI segmentation: state of the art and future directions. *Journal of digital imaging* 30, 4 (2017), 449–459.
- [4] Manal ALAmir and Manal AlGhamdi. 2022. The Role of Generative Adversarial Network in Medical Image Analysis: An in-depth survey. *ACM Computing Surveys (CSUR)* (2022).
- [5] Hazrat Ali, Rafiul Biswas, Farida Ali, Uzair Shah, Asma Alamgir, Osama Mousa, and Zubair Shah. 2022. The role of generative adversarial networks in brain MRI: a scoping review. *Insights into Imaging* 13, 1 (2022), 1–15.
- [6] Sina Amirrajab, Samaneh Abbasi-Sureshjani, Yasmina Al Khalil, Cristian Lorenz, Juergen Weese, Josien Pluim, and Marcel Breeuwer. 2020. Xcat-gan for synthesizing 3d consistent labeled cardiac mr images on anatomically variable xcat phantoms. In *International Conference on Medical Image Computing and Computer-Assisted Intervention*. Springer, 128–137.
- [7] Alexander Andreopoulos and John K Tsotsos. 2008. Efficient and generalizable statistical models of shape and appearance for analysis of cardiac MRI. *Medical image analysis* 12, 3 (2008), 335–357.
- [8] Martin Arjovsky, Soumith Chintala, and Léon Bottou. 2017. Wasserstein generative adversarial networks. In *International conference on machine learning*. PMLR, 214–223.
- [9] Spyridon Bakas, Hamed Akbari, Aristeidis Sotiras, Michel Bilello, Martin Rozycki, Justin S Kirby, John B Freymann, Keyvan Farahani, and Christos Davatzikos. 2017. Advancing the cancer genome atlas glioma MRI collections with expert segmentation labels and radiomic features. *Scientific data* 4, 1 (2017), 1–13.
- [10] Guha Balakrishnan, Amy Zhao, Mert R Sabuncu, John Guttag, and Adrian V Dalca. 2018. An unsupervised learning model for deformable medical image registration. In *Proceedings of the IEEE conference on computer vision and pattern recognition*. 9252–9260.
- [11] Guha Balakrishnan, Amy Zhao, Mert R Sabuncu, John Guttag, and Adrian V Dalca. 2019. VoxelMorph: a learning framework for deformable medical image registration. *IEEE transactions on medical imaging* 38, 8 (2019), 1788–1800.
- [12] Berke Doga Basaran, Mengyun Qiao, Paul M Matthews, and Wenjia Bai. 2022. Subject-specific lesion generation and pseudo-healthy synthesis for multiple sclerosis brain images. In *International Workshop on Simulation and Synthesis in Medical Imaging*. Springer, 1–11.
- [13] Olivier Bernard, Alain Lalonde, Clement Zotti, Frederick Cervenansky, Xin Yang, Pheng-Ann Heng, Irem Cetin, Karim Lekadir, Oscar Camara, Miguel Angel Gonzalez Ballester, et al. 2018. Deep learning techniques for automatic MRI cardiac multi-structures segmentation and diagnosis: is the problem solved? *IEEE transactions on medical imaging* 37, 11 (2018), 2514–2525.
- [14] Carlo Biffi, Ozan Oktay, Giacomo Tarroni, Wenjia Bai, Antonio De Marvao, Georgia Doumou, Martin Rajchl, Reem Bedair, Sanjay Prasad, Stuart Cook, et al. 2018. Learning interpretable anatomical features through deep generative models: Application to cardiac remodeling. In *International conference on medical image computing and computer-assisted intervention*. Springer, 464–471.
- [15] Ali Borji. 2019. Pros and cons of gan evaluation measures. *Computer Vision and Image Understanding* 179 (2019), 41–65.
- [16] Hervé Bourlard and Yves Kamp. 1988. Auto-association by multilayer perceptrons and singular value decomposition. *Biological cybernetics* 59, 4 (1988), 291–294.
- [17] Mariana Bustamante, Federica Viola, Jan Engvall, Carl-Johan Carlhäll, and Tino Ebbers. 2022. Automatic Time-Resolved Cardiovascular Segmentation of 4D Flow MRI Using Deep Learning. *Journal of Magnetic Resonance Imaging* (2022).
- [18] Sihong Chen, Kai Ma, and Yefeng Zheng. 2019. Med3d: Transfer learning for 3d medical image analysis. *arXiv preprint arXiv:1904.00625* (2019).
- [19] Wei Chen, Boqiang Liu, Suting Peng, Jiawei Sun, and Xu Qiao. 2018. S3D-UNet: separable 3D U-Net for brain tumor segmentation. In *International MICCAI Brainlesion Workshop*. Springer, 358–368.
- [20] Yicheng Chen, Angela Jakary, Sivakami Avadiappan, Christopher P Hess, and Janine M Lupo. 2020. QSMGAN: improved quantitative susceptibility mapping using 3D generative adversarial networks with increased receptive field. *NeuroImage* 207 (2020), 116389.
- [21] Yizhou Chen, Xu-Hua Yang, Zihan Wei, Ali Asghar Heidari, Nenggan Zheng, Zhicheng Li, Huiling Chen, Haigen Hu, Qianwei Zhou, and Qiu Guan. 2022. Generative adversarial networks in medical image augmentation: a review. *Computers in Biology and Medicine* (2022), 105382.
- [22] Kyunghyun Cho, B van Merriënboer, Caglar Gulcehre, F Bougares, H Schwenk, and Yoshua Bengio. 2014. Learning phrase representations using RNN encoder-decoder for statistical machine translation. In *Conference on Empirical Methods in Natural Language Processing (EMNLP 2014)*.

- [23] Yunjey Choi, Minje Choi, Munyoung Kim, Jung-Woo Ha, Sunghun Kim, and Jaegul Choo. 2018. Stargan: Unified generative adversarial networks for multi-domain image-to-image translation. In *Proceedings of the IEEE conference on computer vision and pattern recognition*. 8789–8797.
- [24] Chee Keong Chong and Eric Tatt Wei Ho. 2021. Synthesis of 3D MRI brain images with shape and texture generative adversarial deep neural networks. *IEEE Access* 9 (2021), 64747–64760.
- [25] Gary E Christensen, Xiujuan Geng, Jon G Kuhl, Joel Bruss, Thomas J Grabowski, Imran A Pirwani, Michael W Vannier, John S Allen, and Hanna Damasio. 2006. Introduction to the non-rigid image registration evaluation project (NIREP). In *International workshop on biomedical image registration*. Springer, 128–135.
- [26] Hyungjin Chung, Eunju Cha, Leonard Sunwoo, and Jong Chul Ye. 2021. Two-stage deep learning for accelerated 3D time-of-flight MRA without matched training data. *Medical Image Analysis* 71 (2021), 102047.
- [27] Özgün Çiçek, Ahmed Abdulkadir, Soeren S Lienkamp, Thomas Brox, and Olaf Ronneberger. 2016. 3D U-Net: learning dense volumetric segmentation from sparse annotation. In *International conference on medical image computing and computer-assisted intervention*. Springer, 424–432.
- [28] Marco Domenico Cirillo, David Abramian, and Anders Eklund. 2020. Vox2Vox: 3D-GAN for brain tumour segmentation. In *International MICCAI Brainlesion Workshop*. Springer, 274–284.
- [29] Chris A Cocosco, Vasken Kollokian, Remi K-S Kwan, G Bruce Pike, and Alan C Evans. 1997. Brainweb: Online interface to a 3D MRI simulated brain database. In *NeuroImage*. Citeseer.
- [30] Ronan Collobert, Jason Weston, Léon Bottou, Michael Karlen, Koray Kavukcuoglu, and Pavel Kuksa. 2011. Natural language processing (almost) from scratch. *Journal of machine learning research* 12, ARTICLE (2011), 2493–2537.
- [31] Olivier Commowick, Frédéric Cervenansky, and Roxana Ameli. 2016. MSSEG challenge proceedings: multiple sclerosis lesions segmentation challenge using a data management and processing infrastructure. In *Miccai*.
- [32] ADHD-200 consortium. 2012. The ADHD-200 consortium: a model to advance the translational potential of neuroimaging in clinical neuroscience. *Frontiers in systems neuroscience* 6 (2012), 62.
- [33] Alexander Dagley, Molly LaPoint, Willem Huijbers, Trey Hedden, Donald G McLaren, Jasmeer P Chatwal, Kathryn V Papp, Rebecca E Amariglio, Deborah Blacker, Dorene M Rentz, et al. 2017. Harvard aging brain study: dataset and accessibility. *NeuroImage* 144 (2017), 255–258.
- [34] Onat Dalmaz, Mahmut Yurt, and Tolga Çukur. 2021. ResViT: Residual vision transformers for multi-modal medical image synthesis. *arXiv preprint arXiv:2106.16031* (2021).
- [35] Salman UH Dar, Mahmut Yurt, Levent Karacan, Aykut Erdem, Erkut Erdem, and Tolga Cukur. 2019. Image synthesis in multi-contrast MRI with conditional generative adversarial networks. *IEEE transactions on medical imaging* 38, 10 (2019), 2375–2388.
- [36] IXI Dataset. 2010. *IXI brain development homepage*. <https://brain-development.org/ixi-dataset/>
- [37] Annemarie M den Harder, Jelmer M Wolterink, Martin J Willeminck, Arnold MR Schilham, Pim A de Jong, Ricardo PJ Budde, Hendrik M Nathoe, Ivana Išgum, and Tim Leiner. 2016. Submillisievert coronary calcium quantification using model-based iterative reconstruction: a within-patient analysis. *European journal of radiology* 85, 11 (2016), 2152–2159.
- [38] Jia Deng, Wei Dong, Richard Socher, Li-Jia Li, Kai Li, and Li Fei-Fei. 2009. Imagenet: A large-scale hierarchical image database. In *2009 IEEE conference on computer vision and pattern recognition*. Ieee, 248–255.
- [39] Tribikram Dhar, Nilanjan Dey, Surekha Borra, and R Simon Sherratt. 2023. Challenges of Deep Learning in Medical Image Analysis—Improving Explainability and Trust. *IEEE Transactions on Technology and Society* 4, 1 (2023), 68–75.
- [40] Prafulla Dhariwal and Alexander Nichol. 2021. Diffusion models beat gans on image synthesis. *Advances in Neural Information Processing Systems* 34 (2021), 8780–8794.
- [41] Adriana Di Martino, Chao-Gan Yan, Qingyang Li, Erin Denio, Francisco X Castellanos, Kaat Alaerts, Jeffrey S Anderson, Michal Assaf, Susan Y Bookheimer, Mirella Dapretto, et al. 2014. The autism brain imaging data exchange: towards a large-scale evaluation of the intrinsic brain architecture in autism. *Molecular psychiatry* 19, 6 (2014), 659–667.
- [42] Suyu Dong, Gongning Luo, Kuanquan Wang, Shaodong Cao, Ashley Mercado, Olga Shmuilovich, Henggui Zhang, and Shuo Li. 2018. VoxelAtlasGAN: 3D left ventricle segmentation on echocardiography with atlas guided generation and voxel-to-voxel discrimination. In *International Conference on Medical Image Computing and Computer-Assisted Intervention*. Springer, 622–629.
- [43] Hossam El-Rewaify, Ulf Neisius, Jennifer Mancio, Selcuk Kucukseymen, Jennifer Rodriguez, Amanda Paskavitz, Bjoern Menze, and Reza Nezafat. 2020. Deep complex convolutional network for fast reconstruction of 3D late gadolinium enhancement cardiac MRI. *NMR in Biomedicine* 33, 7 (2020), e4312.
- [44] Ahmed Elazab, Changmiao Wang, Syed Jamal Safdar Gardezi, Hongmin Bai, Qingmao Hu, Tianfu Wang, Chunqi Chang, and Baiying Lei. 2020. GP-GAN: Brain tumor growth prediction using stacked 3D generative adversarial networks from longitudinal MR Images. *Neural Networks* 132 (2020), 321–332.

- [45] Thomas Elsken, Jan Hendrik Metzen, and Frank Hutter. 2019. Neural architecture search: A survey. *The Journal of Machine Learning Research* 20, 1 (2019), 1997–2017.
- [46] Yuki Enokiyu, Yutaro Iwamoto, Yen-Wei Chen, and Xian-Hua Han. 2018. Automatic liver segmentation using U-Net with Wasserstein GANs. *Journal of Image and Graphics* 6, 2 (2018), 152–159.
- [47] Patrick Esser, Robin Rombach, and Bjorn Ommer. 2021. Taming transformers for high-resolution image synthesis. In *Proceedings of the IEEE/CVF conference on computer vision and pattern recognition*. 12873–12883.
- [48] Farzan Farnia and Asuman Ozdaglar. 2020. Do GANs always have Nash equilibria?. In *International Conference on Machine Learning*. PMLR, 3029–3039.
- [49] Bruce Fischl. 2012. FreeSurfer. *Neuroimage* 62, 2 (2012), 774–781.
- [50] Yarin Gal and Zoubin Ghahramani. 2016. Dropout as a bayesian approximation: Representing model uncertainty in deep learning. In *international conference on machine learning*. PMLR, 1050–1059.
- [51] Wenshuo Gao, Xiaoguang Zhang, Lei Yang, and Huizhong Liu. 2010. An improved Sobel edge detection. In *2010 3rd International conference on computer science and information technology*, Vol. 5. IEEE, 67–71.
- [52] Ross Girshick. 2015. Fast r-cnn. In *Proceedings of the IEEE international conference on computer vision*. 1440–1448.
- [53] Randy L Gollub, Jody M Shoemaker, Margaret D King, Tonya White, Stefan Ehrlich, Scott R Sponheim, Vincent P Clark, Jessica A Turner, Bryon A Mueller, Vince Magnotta, et al. 2013. The MCIC collection: a shared repository of multi-modal, multi-site brain image data from a clinical investigation of schizophrenia. *Neuroinformatics* 11, 3 (2013), 367–388.
- [54] Lovdeep Gondara. 2016. Medical image denoising using convolutional denoising autoencoders. In *2016 IEEE 16th international conference on data mining workshops (ICDMW)*. IEEE, 241–246.
- [55] Ian Goodfellow, Jean Pouget-Abadie, Mehdi Mirza, Bing Xu, David Warde-Farley, Sherjil Ozair, Aaron Courville, and Yoshua Bengio. 2014. Generative adversarial nets. *Advances in neural information processing systems* 27 (2014).
- [56] Jason L Granstedt, Varun A Kelkar, Weimin Zhou, and Mark A Anastasio. 2021. SlabGAN: a method for generating efficient 3D anisotropic medical volumes using generative adversarial networks. In *Medical Imaging 2021: Image Processing*, Vol. 11596. SPIE, 329–335.
- [57] Alex Graves, Abdel-rahman Mohamed, and Geoffrey Hinton. 2013. Speech recognition with deep recurrent neural networks. In *2013 IEEE international conference on acoustics, speech and signal processing*. Ieee, 6645–6649.
- [58] Karol Gregor, Ivo Danihelka, Andriy Mnih, Charles Blundell, and Daan Wierstra. 2014. Deep autoregressive networks. In *International Conference on Machine Learning*. PMLR, 1242–1250.
- [59] Ishaan Gulrajani, Faruk Ahmed, Martin Arjovsky, Vincent Dumoulin, and Aaron C Courville. 2017. Improved training of wasserstein gans. *Advances in neural information processing systems* 30 (2017).
- [60] Marija Habijan, Irena Galić, Hrvoje Leventić, and Krešimir Romić. 2021. Whole Heart Segmentation Using 3D FM-Pre-ResNet Encoder–Decoder Based Architecture with Variational Autoencoder Regularization. *Applied Sciences* 11, 9 (2021), 3912.
- [61] Changhee Han, Leonardo Rundo, Kohei Murao, Tomoyuki Noguchi, Yuki Shimahara, Zoltán Ádám Milacski, Saori Koshino, Evis Sala, Hideki Nakayama, and Shin’ichi Satoh. 2021. MADGAN: Unsupervised medical anomaly detection GAN using multiple adjacent brain MRI slice reconstruction. *BMC bioinformatics* 22, 2 (2021), 1–20.
- [62] Kaiming He, Xinlei Chen, Saining Xie, Yanghao Li, Piotr Dollár, and Ross Girshick. 2022. Masked autoencoders are scalable vision learners. In *Proceedings of the IEEE/CVF Conference on Computer Vision and Pattern Recognition*. 16000–16009.
- [63] Kaiming He, Georgia Gkioxari, Piotr Dollár, and Ross Girshick. 2017. Mask r-cnn. In *Proceedings of the IEEE international conference on computer vision*. 2961–2969.
- [64] Kaiming He, Xiangyu Zhang, Shaoqing Ren, and Jian Sun. 2016. Deep residual learning for image recognition. In *Proceedings of the IEEE conference on computer vision and pattern recognition*. 770–778.
- [65] Monica Hernandez. 2014. Gauss–Newton inspired preconditioned optimization in large deformation diffeomorphic metric mapping. *Physics in Medicine & Biology* 59, 20 (2014), 6085.
- [66] Martin Heusel, Hubert Ramsauer, Thomas Unterthiner, Bernhard Nessler, and Sepp Hochreiter. 2017. Gans trained by a two time-scale update rule converge to a local nash equilibrium. *Advances in neural information processing systems* 30 (2017).
- [67] GE Hinton. 1994. RS n emel. Autoencoders, minimum description length, and Helmholtz free energy. *J. D. C owan, G. Tesauro, and J. Aspector, editors, dvances in E u ra l l n f ormation rocessin g systems q. Morgan K aufmann P ublishers, San Francisco, C A* (1994).
- [68] Geoffrey Hinton, Li Deng, Dong Yu, George E Dahl, Abdel-rahman Mohamed, Navdeep Jaitly, Andrew Senior, Vincent Vanhoucke, Patrick Nguyen, Tara N Sainath, et al. 2012. Deep neural networks for acoustic modeling in speech recognition: The shared views of four research groups. *IEEE Signal processing magazine* 29, 6 (2012), 82–97.
- [69] Tobias Hinz, Matthew Fisher, Oliver Wang, and Stefan Wermt. 2021. Improved techniques for training single-image gans. In *Proceedings of the IEEE/CVF Winter Conference on Applications of Computer Vision*. 1300–1309.



- [70] Jonathan Ho, Ajay Jain, and Pieter Abbeel. 2020. Denoising diffusion probabilistic models. *Advances in Neural Information Processing Systems* 33 (2020), 6840–6851.
- [71] Jonathan Ho, Chitwan Saharia, William Chan, David J Fleet, Mohammad Norouzi, and Tim Salimans. 2022. Cascaded Diffusion Models for High Fidelity Image Generation. *J. Mach. Learn. Res.* 23 (2022), 47–1.
- [72] S Hodge, C Haselgrove, D Kennedy, and J Frazier. 2009. CANDIShare: A Resource for Pediatric Neuroimaging Data. In *Front. Neuroinform. Conference Abstract: Neuroinformatics*.
- [73] Avram J Holmes, Marisa O Hollinshead, Timothy M O’keefe, Victor I Petrov, Gabriele R Fariello, Lawrence L Wald, Bruce Fischl, Bruce R Rosen, Ross W Mair, Joshua L Roffman, et al. 2015. Brain Genomics Superstruct Project initial data release with structural, functional, and behavioral measures. *Scientific data* 2, 1 (2015), 1–16.
- [74] Sungmin Hong, Razvan Marinescu, Adrian V Dalca, Anna K Bonkhoff, Martin Bretzner, Natalia S Rost, and Polina Golland. 2021. 3d-stylegan: A style-based generative adversarial network for generative modeling of three-dimensional medical images. In *Deep Generative Models, and Data Augmentation, Labelling, and Imperfections*. Springer, 24–34.
- [75] Zhang Hongtao, Yuki Shinomiya, and Shinichi Yoshida. 2020. 3D brain MRI reconstruction based on 2D super-resolution technology. In *2020 IEEE international conference on systems, man, and cybernetics (SMC)*. IEEE, 18–23.
- [76] Benjamin Hotter, Sandra Pittl, Martin Ebinger, Gabriele Oepen, Kati Jegzentis, Kohsuke Kudo, Michal Rozanski, Wolf U Schmidt, Peter Brunecker, Chao Xu, et al. 2009. Prospective study on the mismatch concept in acute stroke patients within the first 24 h after symptom onset-1000Plus study. *BMC neurology* 9, 1 (2009), 1–8.
- [77] Yutai Hou, Yongkui Lai, Yushan Wu, Wanxiang Che, and Ting Liu. 2021. Few-shot learning for multi-label intent detection. In *Proceedings of the AAAI Conference on Artificial Intelligence*, Vol. 35. 13036–13044.
- [78] Yawen Huang, Feng Zheng, Runmin Cong, Weilin Huang, Matthew R Scott, and Ling Shao. 2020. Mcmt-gan: multi-task coherent modality transferable gan for 3d brain image synthesis. *IEEE Transactions on Image Processing* 29 (2020), 8187–8198.
- [79] Ahmed Iqbal, Muhammad Sharif, Mussarat Yasmin, Mudassar Raza, and Shabib Aftab. 2022. Generative adversarial networks and its applications in the biomedical image segmentation: a comprehensive survey. *International Journal of Multimedia Information Retrieval* (2022), 1–36.
- [80] iSeg 2017. 2022. 6-month infant MRI brain segmentation. <https://iseg2017.web.unc.edu/reference/>
- [81] Phillip Isola, Jun-Yan Zhu, Tinghui Zhou, and Alexei A Efros. 2017. Image-to-image translation with conditional adversarial networks. In *Proceedings of the IEEE conference on computer vision and pattern recognition*. 1125–1134.
- [82] Max Jaderberg, Karen Simonyan, Andrew Zisserman, et al. 2015. Spatial transformer networks. *Advances in neural information processing systems* 28 (2015).
- [83] Jiwoong J Jeong, Amara Tariq, Tobiloba Adejumo, Hari Trivedi, Judy W Gichoya, and Imon Banerjee. 2022. Systematic review of generative adversarial networks (gans) for medical image classification and segmentation. *Journal of Digital Imaging*, 1–16.
- [84] Shuiwang Ji, Wei Xu, Ming Yang, and Kai Yu. 2012. 3D convolutional neural networks for human action recognition. *IEEE transactions on pattern analysis and machine intelligence* 35, 1 (2012), 221–231.
- [85] Thomas Joyce and Sebastian Kozerke. 2019. 3D medical image synthesis by factorised representation and deformable model learning. In *International Workshop on Simulation and Synthesis in Medical Imaging*. Springer, 110–119.
- [86] Tero Karras, Timo Aila, Samuli Laine, and Jaakko Lehtinen. 2017. Progressive growing of gans for improved quality, stability, and variation. *arXiv preprint arXiv:1710.10196* (2017).
- [87] Tero Karras, Samuli Laine, and Timo Aila. 2019. A style-based generator architecture for generative adversarial networks. In *Proceedings of the IEEE/CVF conference on computer vision and pattern recognition*. 4401–4410.
- [88] Tero Karras, Samuli Laine, Miika Aittala, Janne Hellsten, Jaakko Lehtinen, and Timo Aila. 2020. Analyzing and improving the image quality of stylegan. In *Proceedings of the IEEE/CVF conference on computer vision and pattern recognition*. 8110–8119.
- [89] Salome Kazemina, Christoph Baur, Arjan Kuijper, Bram van Ginneken, Nassir Navab, Shadi Albarqouni, and Anirban Mukhopadhyay. 2020. GANs for medical image analysis. *Artificial Intelligence in Medicine* 109 (2020), 101938.
- [90] Jacob Devlin Ming-Wei Chang Kenton and Lee Kristina Toutanova. 2019. BERT: Pre-training of Deep Bidirectional Transformers for Language Understanding. In *Proceedings of NAACL-HLT*. 4171–4186.
- [91] Boah Kim and Jong Chul Ye. 2022. Diffusion Deformable Model for 4D Temporal Medical Image Generation. *arXiv preprint arXiv:2206.13295* (2022).
- [92] Diederik P Kingma and Max Welling. 2013. Auto-encoding variational bayes. *arXiv preprint arXiv:1312.6114* (2013).
- [93] Arno Klein, Satrajit S Ghosh, Forrest S Bao, Joachim Giard, Yrjö Häme, Eliezer Stavsky, Noah Lee, Brian Rossa, Martin Reuter, Elias Chaibub Neto, et al. 2017. Mindboggling morphometry of human brains. *PLoS computational biology* 13, 2 (2017), e1005350.
- [94] Martin Kolarik, Radim Burget, Carlos M Travieso-Gonzalez, and Jan Kocica. 2021. Planar 3D Transfer Learning for End to End Unimodal MRI Unbalanced Data Segmentation. In *2020 25th International Conference on Pattern Recognition (ICPR)*. IEEE, 6051–6058.



- [95] Okan Kopuklu, Neslihan Kose, Ahmet Gunduz, and Gerhard Rigoll. 2019. Resource efficient 3d convolutional neural networks. In *Proceedings of the IEEE/CVF International Conference on Computer Vision Workshops*. 0–0.
- [96] Julian Krebs, Hervé Delingette, Nicholas Ayache, and Tommaso Mansi. 2021. Learning a generative motion model from image sequences based on a latent motion matrix. *IEEE Transactions on Medical Imaging* 40, 5 (2021), 1405–1416.
- [97] Alex Krizhevsky, Ilya Sutskever, and Geoffrey E Hinton. 2012. Imagenet classification with deep convolutional neural networks. *Advances in neural information processing systems* 25 (2012).
- [98] KR Kruthika, HD Maheshappa, Alzheimer’s Disease Neuroimaging Initiative, et al. 2019. CBIR system using Capsule Networks and 3D CNN for Alzheimer’s disease diagnosis. *Informatics in Medicine Unlocked* 14 (2019), 59–68.
- [99] Hugo J Kuijf, J Matthijs Biesbroek, Jeroen De Bresser, Rutger Heinen, Simon Andermatt, Mariana Bento, Matt Berseth, Mikhail Belyaev, M Jorge Cardoso, Adria Casamitjana, et al. 2019. Standardized assessment of automatic segmentation of white matter hyperintensities and results of the WMH segmentation challenge. *IEEE transactions on medical imaging* 38, 11 (2019), 2556–2568.
- [100] Gihyun Kwon, Chihye Han, and Dae-shik Kim. 2019. Generation of 3D brain MRI using auto-encoding generative adversarial networks. In *International Conference on Medical Image Computing and Computer-Assisted Intervention*. Springer, 118–126.
- [101] Pamela J LaMontagne, Tammie LS Benzinger, John C Morris, Sarah Keefe, Russ Hornbeck, Chengjie Xiong, Elizabeth Grant, Jason Hassenstab, Krista Moulder, Andrei G Vlassenko, et al. 2019. OASIS-3: longitudinal neuroimaging, clinical, and cognitive dataset for normal aging and Alzheimer disease. *MedRxiv* (2019).
- [102] Haoyu Lan, Arthur W Toga, Farshid Sepehrband, Alzheimer Disease Neuroimaging Initiative, et al. 2020. SC-GAN: 3D self-attention conditional GAN with spectral normalization for multi-modal neuroimaging synthesis. *bioRxiv* (2020).
- [103] Hugo Larochelle and Iain Murray. 2011. The neural autoregressive distribution estimator. In *Proceedings of the fourteenth international conference on artificial intelligence and statistics*. JMLR Workshop and Conference Proceedings, 29–37.
- [104] Yann LeCun. 1987. PhD thesis: Modeles connexionnistes de l’apprentissage (connectionist learning models). (1987).
- [105] Yann LeCun, Léon Bottou, Yoshua Bengio, and Patrick Haffner. 1998. Gradient-based learning applied to document recognition. *Proc. IEEE* 86, 11 (1998), 2278–2324.
- [106] Jihyun Lee, Minhyuk Sung, Hyunjin Kim, and Tae-Kyun Kim. 2022. Pop-Out Motion: 3D-Aware Image Deformation via Learning the Shape Laplacian. In *Proceedings of the IEEE/CVF Conference on Computer Vision and Pattern Recognition*. 18532–18541.
- [107] Michael M Lell and Marc Kachelrieß. 2020. Recent and upcoming technological developments in computed tomography: high speed, low dose, deep learning, multienergy. *Investigative radiology* 55, 1 (2020), 8–19.
- [108] Žiga Lesjak, Alfiia Galimzianova, Aleš Koren, Matej Lukin, Franjo Pernuš, Boštjan Likar, and Žiga Špiclin. 2018. A novel public MR image dataset of multiple sclerosis patients with lesion segmentations based on multi-rater consensus. *Neuroinformatics* 16, 1 (2018), 51–63.
- [109] Chuan Li and Michael Wand. 2016. Precomputed real-time texture synthesis with markovian generative adversarial networks. In *European conference on computer vision*. Springer, 702–716.
- [110] Shuailin Li, Chuyi Zhang, and Xuming He. 2020. Shape-aware semi-supervised 3D semantic segmentation for medical images. In *International Conference on Medical Image Computing and Computer-Assisted Intervention*. Springer, 552–561.
- [111] Haofu Liao, Yucheng Tang, Gareth Funka-Lea, Jiebo Luo, and Shaohua Kevin Zhou. 2018. More knowledge is better: Cross-modality volume completion and 3D+ 2D segmentation for intracardiac echocardiography contouring. In *International Conference on Medical Image Computing and Computer-Assisted Intervention*. Springer, 535–543.
- [112] Sook-Lei Liew, Julia M Anglin, Nick W Banks, Matt Sondag, Kaori L Ito, Hosung Kim, Jennifer Chan, Joyce Ito, Connie Jung, Nima Khoshab, et al. 2018. A large, open source dataset of stroke anatomical brain images and manual lesion segmentations. *Scientific data* 5, 1 (2018), 1–11.
- [113] Wanyun Lin. 2020. Synthesizing missing data using 3D reversible GAN for alzheimer’s disease. In *Proceedings of the 2020 international symposium on artificial intelligence in medical sciences*. 208–213.
- [114] Wanyun Lin, Weiming Lin, Gang Chen, Hejun Zhang, Qinquan Gao, Yechong Huang, Tong Tong, Min Du, and Alzheimer’s Disease Neuroimaging Initiative. 2021. Bidirectional mapping of brain MRI and PET with 3D reversible GAN for the diagnosis of Alzheimer’s disease. *Frontiers in Neuroscience* 15 (2021), 646013.
- [115] Jing Liu, Pengyu Yin, Xiaohui Wang, Wei Yang, and Kun Cheng. 2019. Glioma subregions segmentation with a discriminative adversarial regularized 3D U-net. In *Proceedings of the Third International Symposium on Image Computing and Digital Medicine*. 269–273.
- [116] Ming-Yu Liu, Xun Huang, Arun Mallya, Tero Karras, Timo Aila, Jaakko Lehtinen, and Jan Kautz. 2019. Few-shot unsupervised image-to-image translation. In *Proceedings of the IEEE/CVF international conference on computer vision*. 10551–10560.

- [117] Shengfeng Liu, Yi Wang, Xin Yang, Baiying Lei, Li Liu, Shawn Xiang Li, Dong Ni, and Tianfu Wang. 2019. Deep learning in medical ultrasound analysis: a review. *Engineering* 5, 2 (2019), 261–275.
- [118] Xiao Liu, Fanjin Zhang, Zhenyu Hou, Li Mian, Zhaoyu Wang, Jing Zhang, and Jie Tang. 2021. Self-supervised learning: Generative or contrastive. *IEEE Transactions on Knowledge and Data Engineering* (2021).
- [119] Yanbin Liu, Girish Dwivedi, Farid Boussaid, Frank Sanfilippo, Makoto Yamada, and Mohammed Bennamoun. 2023. Inflating 2D Convolution Weights for Efficient Generation of 3D Medical Images. *Computer Methods and Programs in Biomedicine* (2023), 107685.
- [120] Y Liu, J Lee, M Park, S Kim, E Yang, SJ Hwang, and Y Yang. 2019. Learning to propagate labels: Transductive propagation network for few-shot learning. In *7th International Conference on Learning Representations, ICLR 2019*.
- [121] Yilin Liu, Brendon M Nacewicz, Gengyan Zhao, Nagesh Adluru, Gregory R Kirk, Peter A Ferrazzano, Martin A Styner, and Andrew L Alexander. 2020. A 3D fully convolutional neural network with top-down attention-guided refinement for accurate and robust automatic segmentation of amygdala and its subnuclei. *Frontiers in Neuroscience* 14 (2020), 260.
- [122] Zhihua Liu, Lei Tong, Long Chen, Zheheng Jiang, Feixiang Zhou, Qianni Zhang, Xiangrong Zhang, Yaochu Jin, and Huiyu Zhou. 2022. Deep learning based brain tumor segmentation: a survey. *Complex & Intelligent Systems* (2022), 1–26.
- [123] Alexander Selvikvåg Lundervold and Arvid Lundervold. 2019. An overview of deep learning in medical imaging focusing on MRI. *Zeitschrift für Medizinische Physik* 29, 2 (2019), 102–127.
- [124] Oskar Maier, Bjoern H Menze, Janina von der Gabelntz, Levin Häni, Mattias P Heinrich, Matthias Liebrand, Stefan Winzeck, Abdul Basit, Paul Bentley, Liang Chen, et al. 2017. ISLES 2015-A public evaluation benchmark for ischemic stroke lesion segmentation from multispectral MRI. *Medical image analysis* 35 (2017), 250–269.
- [125] Daniel S Marcus, Tracy H Wang, Jamie Parker, John G Csernansky, John C Morris, and Randy L Buckner. 2007. Open Access Series of Imaging Studies (OASIS): cross-sectional MRI data in young, middle aged, nondemented, and demented older adults. *Journal of cognitive neuroscience* 19, 9 (2007), 1498–1507.
- [126] Kenneth Marek, Danna Jennings, Shirley Lasch, Andrew Siderowf, Caroline Tanner, Tanya Simuni, Chris Coffey, Karl Kieburtz, Emily Flagg, Sohini Chowdhury, et al. 2011. The Parkinson progression marker initiative (PPMI). *Progress in neurobiology* 95, 4 (2011), 629–635.
- [127] Adriënne M Mendrik, Koen L Vincken, Hugo J Kuijf, Marcel Breeuwer, Willem H Bouvy, Jeroen De Bresser, Amir Alansary, Marleen De Bruijne, Aaron Carass, Ayman El-Baz, et al. 2015. MRBrainS challenge: online evaluation framework for brain image segmentation in 3T MRI scans. *Computational intelligence and neuroscience* 2015 (2015).
- [128] Tomáš Mikolov, Anoop Deoras, Daniel Povey, Lukáš Burget, and Jan Černocký. 2011. Strategies for training large scale neural network language models. In *2011 IEEE Workshop on Automatic Speech Recognition & Understanding*. IEEE, 196–201.
- [129] Fausto Milletari, Nassir Navab, and Seyed-Ahmad Ahmadi. 2016. V-net: Fully convolutional neural networks for volumetric medical image segmentation. In *2016 fourth international conference on 3D vision (3DV)*. IEEE, 565–571.
- [130] Mehdi Mirza and Simon Osindero. 2014. Conditional generative adversarial nets. *arXiv preprint arXiv:1411.1784* (2014).
- [131] Anish Mittal, Rajiv Soundararajan, and Alan C Bovik. 2012. Making a “completely blind” image quality analyzer. *IEEE Signal processing letters* 20, 3 (2012), 209–212.
- [132] Arnab Kumar Mondal, Jose Dolz, and Christian Desrosiers. 2018. Few-shot 3d multi-modal medical image segmentation using generative adversarial learning. *arXiv preprint arXiv:1810.12241* (2018).
- [133] NAMIC Multimodality. 2022. *NAMIC Multimodality dataset download link*. <https://insight-journal.org/midas/collection/view/190>
- [134] Matthias A Mutke, Vince I Madai, Federico C von Samson-Himmelstjerna, Olivier Zaro Weber, Gajanan S Revankar, Steve Z Martin, Katharina L Stengl, Miriam Bauer, Stefan Hetzer, Matthias Günther, et al. 2014. Clinical evaluation of an arterial-spin-labeling product sequence in steno-occlusive disease of the brain. *PLoS One* 9, 2 (2014), e87143.
- [135] Andriy Myronenko. 2018. 3D MRI brain tumor segmentation using autoencoder regularization. In *International MICCAI Brainlesion Workshop*. Springer, 311–320.
- [136] Yang Nan, Javier Del Ser, Simon Walsh, Carola Schönlieb, Michael Roberts, Ian Selby, Kit Howard, John Owen, Jon Neville, Julien Guiot, et al. 2022. Data harmonisation for information fusion in digital healthcare: A state-of-the-art systematic review, meta-analysis and future research directions. *Information Fusion* 82 (2022), 99–122.
- [137] S Niyas, SJ Pawan, M Anand Kumar, and Jeny Rajan. 2022. Medical image segmentation with 3D convolutional neural networks: A survey. *Neurocomputing* 493 (2022), 397–413.
- [138] Robert S Oakes, Troy J Badger, Eugene G Kholmovski, Nazem Akoum, Nathan S Burgon, Eric N Fish, Joshua JE Blauer, Swati N Rao, Edward VR DiBella, Nathan M Segerson, et al. 2009. Detection and quantification of left atrial structural remodeling with delayed-enhancement magnetic resonance imaging in patients with atrial fibrillation. *Circulation* 119, 13 (2009), 1758–1767.

- [139] Augustus Odena, Christopher Olah, and Jonathon Shlens. 2017. Conditional image synthesis with auxiliary classifier gans. In *International conference on machine learning*. PMLR, 2642–2651.
- [140] Utkarsh Ojha, Yijun Li, Jingwan Lu, Alexei A Efros, Yong Jae Lee, Eli Shechtman, and Richard Zhang. 2021. Few-shot image generation via cross-domain correspondence. In *Proceedings of the IEEE/CVF Conference on Computer Vision and Pattern Recognition*. 10743–10752.
- [141] Cheng Ouyang, Carlo Biffi, Chen Chen, Turkyay Kart, Huaqi Qiu, and Daniel Rueckert. 2022. Self-supervised Learning for Few-shot Medical Image Segmentation. *IEEE Transactions on Medical Imaging* (2022).
- [142] Muzaffer Özbey, Mahmut Yurt, Salman Ul Hassan Dar, and Tolga Çukur. 2020. Three dimensional mr image synthesis with progressive generative adversarial networks. *arXiv preprint arXiv:2101.05218* (2020).
- [143] Yongsheng Pan, Mingxia Liu, Chunfeng Lian, Tao Zhou, Yong Xia, and Dinggang Shen. 2018. Synthesizing missing PET from MRI with cycle-consistent generative adversarial networks for Alzheimer’s disease diagnosis. In *International conference on medical image computing and computer-assisted intervention*. Springer, 455–463.
- [144] Gabriele Paolacci, Jesse Chandler, and Panagiotis G Ipeirotis. 2010. Running experiments on amazon mechanical turk. *Judgment and Decision making* 5, 5 (2010), 411–419.
- [145] Nick Pawlowski, Daniel Coelho de Castro, and Ben Glocker. 2020. Deep structural causal models for tractable counterfactual inference. *Advances in Neural Information Processing Systems* 33 (2020), 857–869.
- [146] Bo Peng, Bingzheng Liu, Yi Bin, Lili Shen, and Jianjun Lei. 2021. Multi-Modality MR Image Synthesis via Confidence-Guided Aggregation and Cross-Modality Refinement. *IEEE Journal of Biomedical and Health Informatics* 26, 1 (2021), 27–35.
- [147] Suting Peng, Wei Chen, Jiawei Sun, and Boqiang Liu. 2020. Multi-scale 3d u-nets: an approach to automatic segmentation of brain tumor. *International Journal of Imaging Systems and Technology* 30, 1 (2020), 5–17.
- [148] Guim Perarnau, Joost Van De Weijer, Bogdan Raducanu, and Jose M Álvarez. 2016. Invertible conditional gans for image editing. *arXiv preprint arXiv:1611.06355* (2016).
- [149] Harry A Pierson and Michael S Gashler. 2017. Deep learning in robotics: a review of recent research. *Advanced Robotics* 31, 16 (2017), 821–835.
- [150] Walter HL Pinaya, Mark S Graham, Robert Gray, Pedro F Da Costa, Petru-Daniel Tudosiu, Paul Wright, Yee H Mah, Andrew D MacKinnon, James T Teo, Rolf Jager, et al. 2022. Fast Unsupervised Brain Anomaly Detection and Segmentation with Diffusion Models. *arXiv preprint arXiv:2206.03461* (2022).
- [151] Walter HL Pinaya, Petru-Daniel Tudosiu, Robert Gray, Geraint Rees, Parashkev Nachev, Sebastien Ourselin, and M Jorge Cardoso. 2022. Unsupervised brain imaging 3D anomaly detection and segmentation with transformers. *Medical Image Analysis* 79 (2022), 102475.
- [152] Guilherme Pombo, Robert Gray, Jorge Cardoso, Sebastien Ourselin, Geraint Rees, John Ashburner, and Parashkev Nachev. 2021. Equitable modelling of brain imaging by counterfactual augmentation with morphologically constrained 3D deep generative models. *arXiv preprint arXiv:2111.14923* (2021).
- [153] Guilherme Pombo, Robert Gray, Thomas Varsavsky, John Ashburner, and Parashkev Nachev. 2019. Bayesian Volumetric Autoregressive generative models for better semisupervised learning. In *International Conference on Medical Image Computing and Computer-Assisted Intervention*. Springer, 429–437.
- [154] Esther Puyol-Antón, Chen Chen, James R Clough, Bram Ruijsink, Baldeep S Sidhu, Justin Gould, Bradley Porter, Marc Elliott, Vishal Mehta, Daniel Rueckert, et al. 2020. Interpretable deep models for cardiac resynchronisation therapy response prediction. In *International Conference on Medical Image Computing and Computer-Assisted Intervention*. Springer, 284–293.
- [155] Xiaoming Qi, Yuting He, Guanyu Yang, Yang Chen, Jian Yang, Wangyag Liu, Yinsu Zhu, Yi Xu, Huazhong Shu, and Shuo Li. 2021. MVSGAN: Spatial-Aware Multi-View CMR Fusion for Accurate 3D Left Ventricular Myocardium Segmentation. *IEEE Journal of Biomedical and Health Informatics* 26, 5 (2021), 2264–2275.
- [156] Mengyun Qiao, Berke Doga Basaran, Huaqi Qiu, Shuo Wang, Yi Guo, Yuanyuan Wang, Paul M Matthews, Daniel Rueckert, and Wenjia Bai. 2022. Generative modelling of the ageing heart with cross-sectional imaging and clinical data. In *International Workshop on Statistical Atlases and Computational Models of the Heart*. Springer, 3–12.
- [157] Mengyun Qiao, Shuo Wang, Huaqi Qiu, Antonio de Marvao, Declan P O’Regan, Daniel Rueckert, and Wenjia Bai. 2023. CHearT: A Conditional Spatio-Temporal Generative Model for Cardiac Anatomy. *arXiv preprint arXiv:2301.13098* (2023).
- [158] Perry Radau, Yingli Lu, Kim Connelly, Gideon Paul, Alexander J Dick, and Graham A Wright. 2009. Evaluation Framework for Algorithms Segmenting Short Axis Cardiac MRI. (07 2009). <https://doi.org/10.54294/g80ruo>
- [159] Siddharth Ramchandran, Gleb Tikhonov, Otto Lönroth, Pekka Tiikkainen, and Harri Lähdesmäki. 2022. Learning Conditional Variational Autoencoders with Missing Covariates. *arXiv preprint arXiv:2203.01218* (2022).
- [160] Ubaldo Ramon, Monica Hernandez, and Elvira Mayordomo. 2022. LDDMM meets GANs: Generative Adversarial Networks for diffeomorphic registration. In *International Workshop on Biomedical Image Registration*. Springer, 18–28.

- [161] Maosong Ran, Jinrong Hu, Yang Chen, Hu Chen, Huaiqiang Sun, Jiliu Zhou, and Yi Zhang. 2019. Denoising of 3D magnetic resonance images using a residual encoder-decoder Wasserstein generative adversarial network. *Medical image analysis* 55 (2019), 165–180.
- [162] Atul Rawal, James McCoy, Danda B Rawat, Brian M Sadler, and Robert St Amant. 2021. Recent advances in trustworthy explainable artificial intelligence: Status, challenges, and perspectives. *IEEE Transactions on Artificial Intelligence* 3, 6 (2021), 852–866.
- [163] Andrew J Reader, Guillaume Corda, Abolfazl Mehranian, Casper da Costa-Luis, Sam Ellis, and Julia A Schnabel. 2020. Deep learning for PET image reconstruction. *IEEE Transactions on Radiation and Plasma Medical Sciences* 5, 1 (2020), 1–25.
- [164] Scott Reed, Zeynep Akata, Xinchun Yan, Lajanugen Logeswaran, Bernt Schiele, and Honglak Lee. 2016. Generative adversarial text to image synthesis. In *International conference on machine learning*. PMLR, 1060–1069.
- [165] Mina Rezaei, Haojin Yang, and Christoph Meinel. 2018. voxel-GAN: adversarial framework for learning imbalanced brain tumor segmentation. In *International MICCAI Brainlesion Workshop*. Springer, 321–333.
- [166] RIRE. 2022. *RIRE dataset*. <https://www.insight-journal.org/rire/>
- [167] Torsten Rohlfing, Robert Brandt, Randolph Menzel, and Calvin R Maurer Jr. 2004. Evaluation of atlas selection strategies for atlas-based image segmentation with application to confocal microscopy images of bee brains. *NeuroImage* 21, 4 (2004), 1428–1442.
- [168] Olaf Ronneberger, Philipp Fischer, and Thomas Brox. 2015. U-net: Convolutional networks for biomedical image segmentation. In *International Conference on Medical image computing and computer-assisted intervention*. Springer, 234–241.
- [169] Mihaela Rosca, Balaji Lakshminarayanan, David Warde-Farley, and Shakir Mohamed. 2017. Variational approaches for auto-encoding generative adversarial networks. *arXiv preprint arXiv:1706.04987* (2017).
- [170] Sara Sabour, Nicholas Frosst, and Geoffrey E Hinton. 2017. Dynamic routing between capsules. *Advances in neural information processing systems* 30 (2017).
- [171] Seyed Sadegh Mohseni Salehi, Deniz Erdogmus, and Ali Gholipour. 2017. Tversky loss function for image segmentation using 3D fully convolutional deep networks. In *International workshop on machine learning in medical imaging*. Springer, 379–387.
- [172] Tim Salimans, Ian Goodfellow, Wojciech Zaremba, Vicki Cheung, Alec Radford, and Xi Chen. 2016. Improved techniques for training gans. *Advances in neural information processing systems* 29 (2016).
- [173] Divya Saxena and Jiannong Cao. 2021. Generative adversarial networks (GANs) challenges, solutions, and future directions. *ACM Computing Surveys (CSUR)* 54, 3 (2021), 1–42.
- [174] Alice Segato, Valentina Corbetta, Marco Di Marzo, Luca Pozzi, and Elena De Momi. 2020. Data augmentation of 3D brain environment using deep convolutional refined auto-encoding alpha GAN. *IEEE Transactions on Medical Robotics and Bionics* 3, 1 (2020), 269–272.
- [175] Jonathan Shapey, Aaron Kujawa, Reuben Dorent, Guotai Wang, Alexis Dimitriadis, Diana Grishchuk, Ian Paddick, Neil Kitchen, Robert Bradford, Shakeel R Saeed, et al. 2021. Segmentation of vestibular schwannoma from MRI, an open annotated dataset and baseline algorithm. *Scientific Data* 8, 1 (2021), 1–6.
- [176] David W Shattuck, Mubeena Mirza, Vitria Adisetiyo, Cornelius Hojatkashani, Georges Salamon, Katherine L Narr, Russell A Poldrack, Robert M Bilder, and Arthur W Toga. 2008. Construction of a 3D probabilistic atlas of human cortical structures. *NeuroImage* 39, 3 (2008), 1064–1080.
- [177] Apoorva Sikka, Jitender Singh Virk, Deepti R Bathula, et al. 2021. MRI to PET Cross-Modality Translation using Globally and Locally Aware GAN (GLA-GAN) for Multi-Modal Diagnosis of Alzheimer’s Disease. *arXiv preprint arXiv:2108.02160* (2021).
- [178] Amber L Simpson, Michela Antonelli, Spyridon Bakas, Michel Bilello, Keyvan Farahani, Bram Van Ginneken, Annette Kopp-Schneider, Bennett A Landman, Geert Litjens, Bjoern Menze, et al. 2019. A large annotated medical image dataset for the development and evaluation of segmentation algorithms. *arXiv preprint arXiv:1902.09063* (2019).
- [179] Robin Simpson, Jennifer Keegan, and David Firmin. 2013. Efficient and reproducible high resolution spiral myocardial phase velocity mapping of the entire cardiac cycle. *Journal of cardiovascular magnetic resonance* 15, 1 (2013), 1–14.
- [180] Robin Simpson, Jennifer Keegan, Peter Gatehouse, Michael Hansen, and David Firmin. 2014. Spiral tissue phase velocity mapping in a breath-hold with non-cartesian SENSE. *Magnetic resonance in medicine* 72, 3 (2014), 659–668.
- [181] Satya P Singh, Lipo Wang, Sukrit Gupta, Haveesh Goli, Parasuraman Padmanabhan, and Balázs Gulyás. 2020. 3D deep learning on medical images: a review. *Sensors* 20, 18 (2020), 5097.
- [182] Jascha Sohl-Dickstein, Eric Weiss, Niru Maheswaranathan, and Surya Ganguli. 2015. Deep unsupervised learning using nonequilibrium thermodynamics. In *International Conference on Machine Learning*. PMLR, 2256–2265.
- [183] Kihyuk Sohn, Honglak Lee, and Xinchun Yan. 2015. Learning structured output representation using deep conditional generative models. *Advances in neural information processing systems* 28 (2015).

- [184] Akash Srivastava, Lazar Valkov, Chris Russell, Michael U Gutmann, and Charles Sutton. 2017. Veegan: Reducing mode collapse in gans using implicit variational learning. *Advances in neural information processing systems* 30 (2017).
- [185] Pooja Subramaniam, Tabea Kossen, Kerstin Ritter, Anja Hennemuth, Kristian Hildebrand, Adam Hilbert, Jan Sobesky, Michelle Livne, Ivana Galinovic, Ahmed A Khalil, et al. 2022. Generating 3D TOF-MRA volumes and segmentation labels using generative adversarial networks. *Medical Image Analysis* 78 (2022), 102396.
- [186] Cathie Sudlow, John Gallacher, Naomi Allen, Valerie Beral, Paul Burton, John Danesh, Paul Downey, Paul Elliott, Jane Green, Martin Landray, et al. 2015. UK biobank: an open access resource for identifying the causes of a wide range of complex diseases of middle and old age. *PLoS medicine* 12, 3 (2015), e1001779.
- [187] Avan Suinesiaputra, Brett R Cowan, Ahmed O Al-Agamy, Mustafa A Elattar, Nicholas Ayache, Ahmed S Fahmy, Ayman M Khalifa, Pau Medrano-Gracia, Marie-Pierre Jolly, Alan H Kadish, et al. 2014. A collaborative resource to build consensus for automated left ventricular segmentation of cardiac MR images. *Medical image analysis* 18, 1 (2014), 50–62.
- [188] Li Sun, Junxiang Chen, Yanwu Xu, Mingming Gong, Ke Yu, and Kayhan Batmanghelich. 2022. Hierarchical Amortized GAN for 3D High Resolution Medical Image Synthesis. *IEEE Journal of Biomedical and Health Informatics* 26, 8 (2022), 3966–3975.
- [189] Niko Sünderhauf, Oliver Brock, Walter Scheirer, Raia Hadsell, Dieter Fox, Jürgen Leitner, Ben Upcroft, Pieter Abbeel, Wolfram Burgard, Michael Milford, et al. 2018. The limits and potentials of deep learning for robotics. *The International journal of robotics research* 37, 4-5 (2018), 405–420.
- [190] Ilya Sutskever, Oriol Vinyals, and Quoc V Le. 2014. Sequence to sequence learning with neural networks. *Advances in neural information processing systems* 27 (2014).
- [191] Song Tao and Jia Wang. 2020. Alleviation of gradient exploding in GANs: Fake can be real. In *Proceedings of the IEEE/CVF Conference on Computer Vision and Pattern Recognition*. 1191–1200.
- [192] Hoang Thanh-Tung and Truyen Tran. 2020. Catastrophic forgetting and mode collapse in gans. In *2020 international joint conference on neural networks (ijcnn)*. IEEE, 1–10.
- [193] Jonathan Tompson, Ross Goroshin, Arjun Jain, Yann LeCun, and Christoph Bregler. 2015. Efficient object localization using convolutional networks. In *Proceedings of the IEEE conference on computer vision and pattern recognition*. 648–656.
- [194] Matthias S Treder, Ryan Codrai, and Kamen A Tsvetanov. 2022. Quality assessment of anatomical MRI images from Generative Adversarial Networks: human assessment and image quality metrics. *Journal of Neuroscience Methods* 374 (2022), 109579.
- [195] Nontawat Tritrong, Pitchaporn Rewatbowornwong, and Supasorn Suwajanakorn. 2021. Repurposing gans for one-shot semantic part segmentation. In *Proceedings of the IEEE/CVF conference on computer vision and pattern recognition*. 4475–4485.
- [196] Faizad Ullah, Shahab U Ansari, Muhammad Hanif, Mohamed Arselene Ayari, Muhammad Enamul Hoque Chowdhury, Amith Abdullah Khandakar, and Muhammad Salman Khan. 2021. Brain MR image enhancement for tumor segmentation using 3D U-Net. *Sensors* 21, 22 (2021), 7528.
- [197] Hristina Uzunova, Sandra Schultz, Heinz Handels, and Jan Ehrhardt. 2019. Unsupervised pathology detection in medical images using conditional variational autoencoders. *International journal of computer assisted radiology and surgery* 14, 3 (2019), 451–461.
- [198] Aaron Van den Oord, Nal Kalchbrenner, Lasse Espeholt, Oriol Vinyals, Alex Graves, et al. 2016. Conditional image generation with pixelcnn decoders. *Advances in neural information processing systems* 29 (2016).
- [199] Aaron Van Den Oord, Oriol Vinyals, et al. 2017. Neural discrete representation learning. *Advances in neural information processing systems* 30 (2017).
- [200] Tycho FA van der Ouderaa and Daniel E Worrall. 2019. Reversible gans for memory-efficient image-to-image translation. In *Proceedings of the IEEE/CVF Conference on Computer Vision and Pattern Recognition*. 4720–4728.
- [201] David C Van Essen, Stephen M Smith, Deanna M Barch, Timothy EJ Behrens, Essa Yacoub, Kamil Ugurbil, Wu-Minn HCP Consortium, et al. 2013. The WU-Minn human connectome project: an overview. *Neuroimage* 80 (2013), 62–79.
- [202] Aaron Van Oord, Nal Kalchbrenner, and Koray Kavukcuoglu. 2016. Pixel recurrent neural networks. In *International conference on machine learning*. PMLR, 1747–1756.
- [203] Ashish Vaswani, Noam Shazeer, Niki Parmar, Jakob Uszkoreit, Llion Jones, Aidan N Gomez, Łukasz Kaiser, and Illia Polosukhin. 2017. Attention is all you need. *Advances in neural information processing systems* 30 (2017).
- [204] Sulaiman Vesal, Andreas Maier, and Nishant Ravikumar. 2020. Fully automated 3d cardiac mri localisation and segmentation using deep neural networks. *Journal of Imaging* 6, 7 (2020), 65.
- [205] Pascal Vincent, Hugo Larochelle, Yoshua Bengio, and Pierre-Antoine Manzagol. 2008. Extracting and composing robust features with denoising autoencoders. In *Proceedings of the 25th international conference on Machine learning*.

- 1096–1103.
- [206] Pascal Vincent, Hugo Larochelle, Isabelle Lajoie, Yoshua Bengio, Pierre-Antoine Manzagol, and Léon Bottou. 2010. Stacked denoising autoencoders: Learning useful representations in a deep network with a local denoising criterion. *Journal of machine learning research* 11, 12 (2010).
- [207] Anna Volokitin, Ertunc Erdil, Neerav Karani, Kerem Can Tezcan, Xiaoran Chen, Luc Van Gool, and Ender Konukoglu. 2020. Modelling the distribution of 3D brain MRI using a 2D slice VAE. In *International Conference on Medical Image Computing and Computer-Assisted Intervention*. Springer, 657–666.
- [208] Chengjia Wang, Giorgos Papanastasiou, Sotirios Tsaftaris, Guang Yang, Calum Gray, David Newby, Gillian Macnaught, and Tom MacGillivray. 2019. TPSDicyc: Improved deformation invariant cross-domain medical image synthesis. In *Machine Learning for Medical Image Reconstruction: Second International Workshop, MLMIR 2019, Held in Conjunction with MICCAI 2019, Shenzhen, China, October 17, 2019, Proceedings 2*. Springer, 245–254.
- [209] Chengjia Wang, Guang Yang, Giorgos Papanastasiou, Sotirios A Tsaftaris, David E Newby, Calum Gray, Gillian Macnaught, and Tom J MacGillivray. 2021. DiCyc: GAN-based deformation invariant cross-domain information fusion for medical image synthesis. *Information Fusion* 67 (2021), 147–160.
- [210] Liansheng Wang, Cong Xie, and Nianyin Zeng. 2019. RP-Net: a 3D convolutional neural network for brain segmentation from magnetic resonance imaging. *IEEE Access* 7 (2019), 39670–39679.
- [211] Xintao Wang, Ke Yu, Shixiang Wu, Jinjin Gu, Yihao Liu, Chao Dong, Yu Qiao, and Chen Change Loy. 2018. Esrgan: Enhanced super-resolution generative adversarial networks. In *Proceedings of the European conference on computer vision (ECCV) workshops*. 0–0.
- [212] Yaqing Wang, Quanming Yao, James T Kwok, and Lionel M Ni. 2020. Generalizing from a few examples: A survey on few-shot learning. *ACM computing surveys (csur)* 53, 3 (2020), 1–34.
- [213] Yan Wang, Biting Yu, Lei Wang, Chen Zu, David S Lalush, Weili Lin, Xi Wu, Jiliu Zhou, Dinggang Shen, and Luping Zhou. 2018. 3D conditional generative adversarial networks for high-quality PET image estimation at low dose. *Neuroimage* 174 (2018), 550–562.
- [214] Yan Wang, Luping Zhou, Biting Yu, Lei Wang, Chen Zu, David S Lalush, Weili Lin, Xi Wu, Jiliu Zhou, and Dinggang Shen. 2018. 3D auto-context-based locality adaptive multi-modality GANs for PET synthesis. *IEEE transactions on medical imaging* 38, 6 (2018), 1328–1339.
- [215] Michael W Weiner, Dallas P Veitch, Paul S Aisen, Laurel A Beckett, Nigel J Cairns, Robert C Green, Danielle Harvey, Clifford R Jack Jr, William Jagust, John C Morris, et al. 2017. The Alzheimer’s Disease Neuroimaging Initiative 3: Continued innovation for clinical trial improvement. *Alzheimer’s & Dementia* 13, 5 (2017), 561–571.
- [216] Jelmer M Wolterink, Tim Leiner, Max A Viergever, and Ivana Išgum. 2017. Generative adversarial networks for noise reduction in low-dose CT. *IEEE transactions on medical imaging* 36, 12 (2017), 2536–2545.
- [217] Tobias Würfl, Florin C Ghesu, Vincent Christlein, and Andreas Maier. 2016. Deep learning computed tomography. In *International conference on medical image computing and computer-assisted intervention*. Springer, 432–440.
- [218] Tian Xia, Agisilaos Chartsias, Sotirios A Tsaftaris, and Alzheimer’s Disease Neuroimaging Initiative. 2019. Consistent brain ageing synthesis. In *Medical Image Computing and Computer Assisted Intervention—MICCAI 2019: 22nd International Conference, Shenzhen, China, October 13–17, 2019, Proceedings, Part IV 22*. Springer, 750–758.
- [219] Haonan Xiao, Xinzhi Teng, Chenyang Liu, Tian Li, Ge Ren, Ruijie Yang, Dinggang Shen, and Jing Cai. 2021. A review of deep learning-based three-dimensional medical image registration methods. *Quantitative Imaging in Medicine and Surgery* 11, 12 (2021), 4895.
- [220] Xiaodan Xing, Javier Del Ser, Yinzhe Wu, Yang Li, Jun Xia, Xu Lei, David Firmin, Peter Gatehouse, and Guang Yang. 2022. HDL: Hybrid Deep Learning for the Synthesis of Myocardial Velocity Maps in Digital Twins for Cardiac Analysis. *IEEE Journal of Biomedical and Health Informatics* (2022).
- [221] Xiaodan Xing, Jiahao Huang, Yang Nan, Yinzhe Wu, Chengjia Wang, Zhifan Gao, Simon Walsh, and Guang Yang. 2022. CS 2: A Controllable and Simultaneous Synthesizer of Images and Annotations with Minimal Human Intervention. In *International Conference on Medical Image Computing and Computer-Assisted Intervention*. Springer, 3–12.
- [222] Xiaodan Xing, Huanjun Wu, Lichao Wang, Iain Stenson, May Yong, Javier Del Ser, Simon Walsh, and Guang Yang. 2022. Non-Imaging Medical Data Synthesis for Trustworthy AI: A Comprehensive Survey. *arXiv preprint arXiv:2209.09239* (2022).
- [223] Xiaodan Xing, Yinzhe Wu, David Firmin, Peter Gatehouse, and Guang Yang. 2022. Synthetic velocity mapping cardiac MRI coupled with automated left ventricle segmentation. In *Medical Imaging 2022: Image Processing*, Vol. 12032. SPIE, 781–785.
- [224] Xiangyu Xiong, Yan Ding, Chuanqi Sun, Zhuoneng Zhang, Xiuhong Guan, Tianjing Zhang, Hao Chen, Hongyan Liu, Zhangbo Cheng, Lei Zhao, et al. 2022. A Cascaded Multi-Task Generative Framework for Detecting Aortic Dissection on 3D Non-contrast-enhanced Computed Tomography. *IEEE Journal of Biomedical and Health Informatics* (2022).
- [225] Zhaohan Xiong, Qing Xia, Zhiqiang Hu, Ning Huang, Cheng Bian, Yefeng Zheng, Sulaiman Vesal, Nishant Ravikumar, Andreas Maier, Xin Yang, et al. 2021. A global benchmark of algorithms for segmenting the left atrium from late

- gadolinium-enhanced cardiac magnetic resonance imaging. *Medical Image Analysis* 67 (2021), 101832.
- [226] Chenchu Xu, Joanne Howey, Pavlo Ohorodnyk, Mike Roth, Heye Zhang, and Shuo Li. 2020. Segmentation and quantification of infarction without contrast agents via spatiotemporal generative adversarial learning. *Medical image analysis* 59 (2020), 101568.
- [227] Chenchu Xu, Lei Xu, Gary Brahm, Heye Zhang, and Shuo Li. 2018. MuTGAN: simultaneous segmentation and quantification of myocardial infarction without contrast agents via joint adversarial learning. In *International Conference on Medical Image Computing and Computer-Assisted Intervention*. Springer, 525–534.
- [228] Chenchu Xu, Lei Xu, Pavlo Ohorodnyk, Mike Roth, Bo Chen, and Shuo Li. 2020. Contrast agent-free synthesis and segmentation of ischemic heart disease images using progressive sequential causal GANs. *Medical image analysis* 62 (2020), 101668.
- [229] Xinchun Yan, Jimei Yang, Kihyuk Sohn, and Honglak Lee. 2016. Attribute2image: Conditional image generation from visual attributes. In *European conference on computer vision*. Springer, 776–791.
- [230] Dong Yang, Bo Liu, Leon Axel, and Dimitris Metaxas. 2018. 3d lv probabilistic segmentation in cardiac mri using generative adversarial network. In *International Workshop on Statistical Atlases and Computational Models of the Heart*. Springer, 181–190.
- [231] Huan Yang, Xianling Lu, Shui-Hua Wang, Zhihai Lu, Jian Yao, Yizhang Jiang, and Pengjiang Qian. 2021. Synthesizing multi-contrast MR images via novel 3D conditional Variational auto-encoding GAN. *Mobile Networks and Applications* 26, 1 (2021), 415–424.
- [232] Jiancheng Yang, Rui Shi, Donglai Wei, Zequan Liu, Lin Zhao, Bilian Ke, Hanspeter Pfister, and Bingbing Ni. 2021. Medmnist v2: A large-scale lightweight benchmark for 2d and 3d biomedical image classification. *arXiv preprint arXiv:2110.14795* (2021).
- [233] Kai Yao, Zixian Su, Kaizhu Huang, Xi Yang, Jie Sun, Amir Hussain, and Frans Coenen. 2022. A novel 3D unsupervised domain adaptation framework for cross-modality medical image segmentation. *IEEE Journal of Biomedical and Health Informatics* (2022).
- [234] Xin Yi, Ekta Walia, and Paul Babyn. 2019. Generative adversarial network in medical imaging: A review. *Medical image analysis* 58 (2019), 101552.
- [235] Biting Yu, Luping Zhou, Lei Wang, Jurgen Fripp, and Pierrick Bourgeat. 2018. 3D cGAN based cross-modality MR image synthesis for brain tumor segmentation. In *2018 IEEE 15th international symposium on biomedical imaging (ISBI 2018)*. IEEE, 626–630.
- [236] Biting Yu, Luping Zhou, Lei Wang, Yinghuan Shi, Jurgen Fripp, and Pierrick Bourgeat. 2019. Ea-GANs: edge-aware generative adversarial networks for cross-modality MR image synthesis. *IEEE transactions on medical imaging* 38, 7 (2019), 1750–1762.
- [237] Biting Yu, Luping Zhou, Lei Wang, Yinghuan Shi, Jurgen Fripp, and Pierrick Bourgeat. 2020. Sample-adaptive gans: Linking global and local mappings for cross-modality mr image synthesis. *IEEE transactions on medical imaging* 39, 7 (2020), 2339–2350.
- [238] Lequan Yu, Shujun Wang, Xiaomeng Li, Chi-Wing Fu, and Pheng-Ann Heng. 2019. Uncertainty-aware self-ensembling model for semi-supervised 3D left atrium segmentation. In *International Conference on Medical Image Computing and Computer-Assisted Intervention*. Springer, 605–613.
- [239] Wenguang Yuan, Jia Wei, Jiabing Wang, Qianli Ma, and Tolga Tasdizen. 2020. Unified generative adversarial networks for multimodal segmentation from unpaired 3D medical images. *Medical Image Analysis* 64 (2020), 101731.
- [240] Mahmut Yurt, Muzaffer Özbey, Salman UH Dar, Berk Tinaz, Kader K Oguz, and Tolga Çukur. 2022. Progressively volumetrized deep generative models for data-efficient contextual learning of MR image recovery. *Medical Image Analysis* 78 (2022), 102429.
- [241] Jure Zbontar, Florian Knoll, Anuroop Sriram, Tullie Murrell, Zhengnan Huang, Matthew J Muckley, Aaron Defazio, Ruben Stern, Patricia Johnson, Mary Bruno, et al. 2018. fastMRI: An open dataset and benchmarks for accelerated MRI. *arXiv preprint arXiv:1811.08839* (2018).
- [242] Dingwen Zhang, Guohai Huang, Qiang Zhang, Jungong Han, Junwei Han, and Yizhou Yu. 2021. Cross-modality deep feature learning for brain tumor segmentation. *Pattern Recognition* 110 (2021), 107562.
- [243] Han Zhang, Tao Xu, Hongsheng Li, Shaoting Zhang, Xiaogang Wang, Xiaolei Huang, and Dimitris N Metaxas. 2017. Stackgan: Text to photo-realistic image synthesis with stacked generative adversarial networks. In *Proceedings of the IEEE international conference on computer vision*. 5907–5915.
- [244] Han Zhang, Tao Xu, Hongsheng Li, Shaoting Zhang, Xiaogang Wang, Xiaolei Huang, and Dimitris N Metaxas. 2018. Stackgan++: Realistic image synthesis with stacked generative adversarial networks. *IEEE transactions on pattern analysis and machine intelligence* 41, 8 (2018), 1947–1962.
- [245] Le Zhang, Ali Gooya, and Alejandro F Frangi. 2017. Semi-supervised assessment of incomplete LV coverage in cardiac MRI using generative adversarial nets. In *International workshop on simulation and synthesis in medical imaging*. Springer, 61–68.



- [246] Xiaoyue Zhang, Weijian Jian, Yu Chen, and Shihting Yang. 2020. Deform-GAN: an unsupervised learning model for deformable registration. *arXiv preprint arXiv:2002.11430* (2020).
- [247] Zizhao Zhang, Lin Yang, and Yefeng Zheng. 2018. Translating and segmenting multimodal medical volumes with cycle-and shape-consistency generative adversarial network. In *Proceedings of the IEEE conference on computer vision and pattern Recognition*. 9242–9251.
- [248] Long Zhao, Zizhao Zhang, Ting Chen, Dimitris Metaxas, and Han Zhang. 2021. Improved transformer for high-resolution gans. *Advances in Neural Information Processing Systems* 34 (2021), 18367–18380.
- [249] Pu Zhao, Hong Pan, and Siyu Xia. 2021. MRI-Trans-GAN: 3D MRI Cross-Modality Translation. In *2021 40th Chinese Control Conference (CCC)*. IEEE, 7229–7234.
- [250] Shengyu Zhao, Tingfung Lau, Ji Luo, I Eric, Chao Chang, and Yan Xu. 2019. Unsupervised 3D end-to-end medical image registration with volume tweening network. *IEEE journal of biomedical and health informatics* 24, 5 (2019), 1394–1404.
- [251] Zhengli Zhao, Sameer Singh, Honglak Lee, Zizhao Zhang, Augustus Odena, and Han Zhang. 2021. Improved consistency regularization for gans. In *Proceedings of the AAAI Conference on Artificial Intelligence*, Vol. 35. 11033–11041.
- [252] Yang Zhou, Zhiwen Yang, Hui Zhang, I Eric, Chao Chang, Yubo Fan, and Yan Xu. 2022. 3D Segmentation Guided Style-based Generative Adversarial Networks for PET Synthesis. *IEEE Transactions on Medical Imaging* (2022).
- [253] Jun-Yan Zhu, Taesung Park, Phillip Isola, and Alexei A Efros. 2017. Unpaired image-to-image translation using cycle-consistent adversarial networks. In *Proceedings of the IEEE international conference on computer vision*. 2223–2232.
- [254] Xingxing Zhu, Zhiwen Huang, Mingyue Ding, and Xuming Zhang. 2022. Non-rigid multi-modal brain image registration based on two-stage generative adversarial nets. *Neurocomputing* 505 (2022), 44–57.
- [255] Zhenyu Zhu, Yiqin Cao, Chenchen Qin, Yi Rao, Di Lin, Qi Dou, Dong Ni, and Yi Wang. 2021. Joint affine and deformable three-dimensional networks for brain MRI registration. *Medical Physics* 48, 3 (2021), 1182–1196.
- [256] Xiahai Zhuang and Juan Shen. 2016. Multi-scale patch and multi-modality atlases for whole heart segmentation of MRI. *Medical image analysis* 31 (2016), 77–87.